Carbohydrate Polymers 329 (2024) 121788

Contents lists available at ScienceDirect

Carbohydrate Polymers

journal homepage: www.elsevier.com/locate/carbpol

Additive manufacturing of wet-spun chitosan/hyaluronic acid scaffolds for biomedical applications

Simona Braccini [a,1], Chong-Bo Chen [b,1], Jeannette Jacqueline Łucejko [a], Francesca Barsotti [a], Claudia Ferrario [a], Guo-Qiang Chen [b], Dario Puppi [a,*]

[a] Department of Chemistry and Industrial Chemistry, University of Pisa, Via Moruzzi 13, 56124 Pisa, Italy
[b] School of Life Sciences, Department of Chemical Engineering, Tsinghua University, Beijing 100084, China

ARTICLE INFO

Keywords:
Chitosan
Hyaluronic acid
Hydrogels
Polyelectrolyte complexes
Additive manufacturing
3D printing

ABSTRACT

Additive manufacturing (AM) holds great potential for processing natural polymer hydrogels into 3D scaffolds exploitable for tissue engineering and in vitro tissue modelling. The aim of this research activity was to assess the suitability of computer-aided wet-spinning (CAWS) for AM of hyaluronic acid (HA)/chitosan (Cs) polyelectrolyte complex (PEC) hydrogels. A post-printing treatment based on HA chemical cross-linking via transesterification with poly(methyl vinyl ether-*alt*-maleic acid) (PMVEMA) was investigated to enhance the structural stability of the developed scaffolds in physiological conditions. PEC formation and the esterification reaction were investigated by infrared spectroscopy, thermogravimetric analysis, evolved gas analysis-mass spectrometry, and differential scanning calorimetry measurements. In addition, variation of PMVEMA concentration in the cross-linking medium was demonstrated to strongly influence scaffold water uptake and its stability in phosphate buffer saline at 37 °C. The in vitro cytocompatibility of the developed hydrogels was demonstrated by employing the murine embryo fibroblast Balb/3T3 clone A31 cell line, highlighting that PMVEMA cross-linking improved scaffold cell colonization. The results achieved demonstrated that the developed hydrogels represent suitable 3D scaffolds for long term cell culture experiments.

1. Introduction

A wide range of polymers derived from natural resources have been explored for biomedical applications in order to exploit their intrinsic biocompatibility and bioactivity, as well as their high potential for sustainable development starting from renewable sources (Morelli et al., 2013). The functional groups of natural macromolecules can endow the resulting biomedical material with specific biofunctionalities, like biological signaling and responsive cell degradation. Among other natural macromolecules investigated in the biomedical field, polysaccharides have gained increasing attention in the past decades thanks to their potential as polymeric matrices for the development of tissue engineering scaffolds and drug release systems (Sood et al., 2021). Various sustainable resources can provide polysaccharides, often as industrial wastes, including plants, animals, and microorganisms, typically with lower extraction and purification costs in comparison to proteins.

Hyaluronic acid (HA) is a linear polysaccharide composed of D-glucuronic acid and *N*-acetyl-D-glucosamine, linked via alternating β-(1 → 4) and β-(1 → 3) glycosidic bonds, constituting the extracellular matrix of several connective tissues. Besides having a structural role, HA interacts with cell receptors and bioactive compounds, such as binding proteins and proteoglycans, influencing angiogenesis and tissue healing processing (Campoccia et al., 1998). HA for biomedical and cosmetic applications is typically extracted from animal tissues, such as rooster comb, bovine synovial fluid, and human umbilical cord. Bacterial fermentation is also extensively investigated and industrially exploited in order to increase the production yield, reproducibility, and sustainability (Yao et al., 2021). Given its good biocompatibility, capability to interact with cell-surface receptors, and unique viscoelastic properties, HA has been employed for applications ranging from the delivery of drugs, such as DNA and other bioactive agents, to tissue engineering and cell encapsulation (Dovedytis et al., 2020; Nitta & Numata, 2013). However, HA high solubility in aqueous physiological fluids limits its application as biomaterial (Campoccia et al., 1998). In addition, in some

* Corresponding author.
E-mail address: dario.puppi@unipi.it (D. Puppi).
[1] These authors contributed equally to the work.

https://doi.org/10.1016/j.carbpol.2024.121788
Received 10 November 2023; Received in revised form 26 December 2023; Accepted 4 January 2024
Available online 9 January 2024

cases a limited cell adhesion has been demonstrated as a consequence of the polyanionic macromolecular structure of HA at a physiological pH (Shu et al., 2003). Therefore, various strategies, including chemical cross-linking, blending with other polymers, and alkyl esterification, have been explored to engineer HA chemical, physical, and biological properties (Puppi et al., 2010).

Chitosan (Cs) is a linear polysaccharide industrially produced mainly from food wastes by deacetylation of chitin, i.e., poly(β-(1–4)-*N*-acetyl-D-glucosamine), extracted from the exoskeleton of crustaceans (Jiménez-Gómez & Cecilia, 2020). A great interest on Cs for biomedical applications stems from its biocompatibility, antibacterial properties, and processing versatility (de Sousa Victor et al., 2020; Notario-Pérez et al., 2022). Indeed, while chitin is not soluble in water and most organic solvents, Cs can be readily solubilized in mild acidic conditions as a consequence of its ammine side groups protonation (pKa ≈ 6.2–6.5) (Wang et al., 2006). For these reasons, Cs has been investigated as a scaffolding material to guide bone regeneration both in vitro and in vivo (Islam et al., 2020), as well as for cartilage engineering given its similar structure to glycine aminoglycan (Zhang et al., 2023). Non-covalent methods based on ionic and hydrogen bond intermolecular interactions can be employed to formulate Cs-based hydrogels with high water absorption capability and long-term stability in physiological media (Dash et al., 2011). In particular, the polycationic form of Cs is able to form a polyelectrolyte complex (PEC) through simple mixing at a controlled pH with different natural polymers, such as alginate and HA, or synthetic polyanions, resulting in hydrogels with tailorable physical-chemical properties and bioactivity (Morelli et al., 2017). For instance, Cs/HA PEC films with different compositions that could swell rapidly at a high ratio and in response to external stimuli were developed (Kim et al., 2004). A study reporting on the development of Cs fibrous scaffolds fabricated by wet-spinning demonstrated that HA coating greatly improved the adhesion, proliferation, and extracellular matrix synthesis of rabbits articular chondrocytes (Yamane et al., 2005). Further studies showed that freeze dried Cs/HA PEC scaffolds well supported the adhesion and proliferation of chondrocytes (Correia et al., 2011), mesenchymal stem cells (Coimbra et al., 2011), and preosteoblasts (Nath et al., 2015). In addition, this kind of scaffold supported the growth of human glioblastoma cells with stem-like properties, able to self-organize into tumoral spheroids suitable for pre-clinical screening of cancer therapeutics (Florczyk et al., 2013), as well as wound healing in rats when loaded with Andrographolide lipid nanocarriers (Sanad & Abdel-Bar, 2017).

Additive manufacturing (AM), also referred to as 3D printing, has been widely investigated for processing natural polymers into 3D hydrogels with a predefined shape and a macroporous structure through a layer-by-layer approach (Li et al., 2020). In comparison to other techniques conventionally applied for hydrogel processing (e.g., freeze drying), AM techniques enable a higher control over the composition and geometrical features of the resulting 3D construct, in terms of reproducibility and design freedom, as well as a higher degree of automation of the relevant production process. In this context, computer-aided wet-spinning (CAWS) enables the extrusion of a hydrogel-forming polymeric mixture directly into a non-solvent bath to obtain 3D scaffolds trough a layered manufacturing process. Originally developed to fabricate scaffolds made of synthetic (Puppi et al., 2012) or natural (Puppi et al., 2020) aliphatic polyesters, CAWS was also employed to process PECs made of Cs and poly(γ-glutamic acid) into 3D porous hydrogels suitable for in vitro pancreatic tumor modelling (Chiellini et al., 2016). However, to the best of the authors' knowledge, this AM approach has not yet been employed for Cs/HA PEC processing. Recent articles investigated the application of other AM approaches to the fabrication of macrostructured hydrogels made of a combination of Cs and HA, but only upon polysaccharides chemical modification before processing or through alternate deposition of Cs and HA filaments without their actual molecular blending (Maiz-Fernández et al., 2021; Suo et al., 2022).

In this context, the here described research activity was aimed at the design and fabrication by CAWS of porous hydrogels based on a PEC between a commercial Cs derived from crustacean shell and a microbial HA. This approach was investigated for the first time as an innovative means for the development of Cs/HA PEC hydrogels with a controlled macroporous structure. The proposed layer-by-layer fabrication process was optimized by investigating the processing conditions for the fabrication of hydrogels with different Cs/HA ratio. In addition, a post-printing treatment process based on HA chemical cross-linking via transesterification with poly(methyl vinyl ether-*alt*-maleic acid) (PMVEMA) was investigated in order to optimize the structural stability of the developed scaffolds in a physiological environment. PMVEMA is a biocompatible copolymer obtained by hydrolysis of the respective FDA-approved anhydride, i.e., poly(methyl vinyl ether-*alt*-maleic anhydride) (Chhabra et al., 2014). Since HA solubilization upon PEC incubation in a physiological medium is a poorly explored topic in the literature, the proposed cross-linking strategy and relevant characterization activities are other important and original aspects of the undertaken study. The additively manufactured scaffolds were characterized by means of FT-IR spectroscopy, water uptake (WU) test, thermogravimetric analysis (TGA), evolved gas analysis-mass spectrometry (EGA-MS), differential scanning calorimetry (DSC), and scanning electron microscopy (SEM). In addition, a preliminary in vitro cell culture experiment was carried out to investigate hydrogels compatibility to the murine embryo fibroblast cell line Balb/3T3 clone A31.

2. Materials and methods

2.1. Materials

Chitosan (Cs, M_w = 50–190 KDa, deacetylation degree of 92 %) and poly(methyl vinyl ether-*alt*-maleic acid) (PMVEMA, $M_w = 2 \times 10^3$ KDa, M_n = 960 KDa) were purchased from Sigma-Aldrich (Milan, Italy). Hyaluronic acid (HA, $M_w = 1 \times 10^3$ KDa) from *Streptococcus zoopidermicus* was supplied by Tsinghua University (Beijing, China). Absolute ethanol (EtOH) and acetic acid were bought from Sigma-Aldrich (Milan, Italy) and used as received.

2.2. Hydrogels fabrication

0.05 g of HA were dissolved in 5 mL of dH_2O (1 % w/v) under vigorous stirring at room temperature for 16 h. A given amount of Cs was added to the prepared HA solution in order to achieve the desired HA/Cs percentage weight ratio (20 to 80 %) and the resulting suspension was left at room temperature under vigorous stirring for 8 h. 50 μL of acetic acid were then added to the suspension and the resulting mixture was left at room temperature under stirring for 2–6 days, depending on composition.

Hydrogels were fabricated by employing a CAWS apparatus previously described (Puppi & Chiellini, 2021). In brief, the desired polymeric mixture was loaded into a 5 mL plastic syringe, fitted with a blunt tip stainless steel needle (gauge 23), that was placed into a syringe pump. The mixture was extruded at a controlled flow rate (F) and deposited layer-by-layer with a controlled velocity (V_{dep}) directly into an EtOH bath. Porous hydrogels with a base size of 12 × 12 mm^2 and two different number of layers (32 or 80) were designed by setting a 0–90° lay-down pattern and a distance between deposition lines (d_{XY}) of 500 μm.

After fabrication, the hydrogels were subjected to different post-printing treatments (Table 1). In particular, the fabricated samples were incubated in a solution of PMVEMA (1–7.5 % w/v) in EtOH for i) 24 h at 65 °C or ii) 5 h at RT with subsequent removal of the solution and sample incubation in an oven at 80 °C for 24 h. After that, the scaffolds were subjected to 3 quick washes in EtOH in order to remove unbound PMVEMA and kept under a fume hood until drying.

Table 1
Post-printing treatment conditions.

Scaffold	Post-printing treatment
HA/Cs	Scaffolds without post-printing treatments
HA/Cs/PMVEMA	Scaffolds incubated in a PMVEMA/EtOH solution at RT for 5 h
HA/Cs/PMVEMA 80 °C	Scaffolds incubated in a PMVEMA/EtOH solution at RT for 5 h and then removed from the solution and kept at 80 °C for 24 h
HA/Cs/PMVEMA 65 °C	Scaffolds incubated in a PMVEMA/EtOH solution at 65 °C for 24 h

2.3. Fourier transform infrared (FT-IR) spectroscopy

FT-IR spectroscopy in attenuated total reflectance mode (FTIR-ATR) analysis was carried out by using a FTIR-Nicolet iS50® instrument (Thermo Fisher scientific, Milan, Italy) equipped with a Smart iTX accessory with diamond crystal, in the range of 4000–600 cm^{-1}, resolution of 2 cm^{-1}. Each spectrum was recorded after 64 scans.

2.4. Water uptake (WU)

To determine hydrogel's WU and stability in physiological conditions, three samples of each scaffold type were incubated in PBS 1× (pH = 7.4) at 37 °C. At specific time points, the samples were collected, dabbed and weighed. The WU at each time point was calculated as:

$$WU = \frac{W_s - W_d}{W_d} \times 100$$

where W_s and W_d are the weight of the swollen and dry scaffold, respectively.

2.5. Thermogravimetric analysis (TGA)

A Q500 instrument (TA Instruments, Milan, Italy) was employed to carry out the analysis under a nitrogen inert atmosphere (60 mL/min), in the range 30–700 °C, by applying a heating rate of 10 °C/min. The temperatures corresponding to maximum points (T_{max}) in the derivative weight vs temperature thermograms were acquired. Each analysis was performed by analyzing three sample replicates for each kind of scaffold.

2.6. Evolved gas analysis (EGA-MS)

The EGA-MS setup included a micro-furnace Multi-Shot Pyrolyzer EGA/Py-3030D (Frontier Lab, Japan), connected to 6890 Gas Chromatograph (Agilent Technologies, USA) equipped with a deactivated stainless steel transfer tube (UADTM-2.5 N, 0.15 mm i.d. × 2.5 m length, Frontier Lab, Japan) and 5973 Agilent Mass Selective Detector. The micro-furnace chamber was programmed to follow a temperature profile: it started at 50 °C and increased the temperature at a rate of 25 °C/min until reaching 700 °C, under a helium flow rate of 1 mL/min (1:20 split ratio). The interface temperature of pyrolyser was maintained at 100 °C higher than the furnace temperature, up to a maximum of 300 °C. The inlet temperature was set at 280 °C, while that of the chromatographic oven was kept at 300 °C. The MS operated in the EI positive mode with an electron energy of 70 eV and scanned the mass-to-charge ratio (m/z) range from 50 to 600. MS temperature conditions were: transfer line at 300 °C, ion source at 230 °C, and the quadrupole at 150 °C. Each sample (about 0.25 mg) was placed in a stainless-steel cup and introduced into the micro-furnace. The resulting gaseous compounds were directly ionized and analyzed over time. The outcome of this process was a total ion thermogram (TIT) representing the volatile products evolved within the investigated range of temperatures.

2.7. Differential scanning calorimetry (DSC)

Samples were characterized under a nitrogen flow rate of 80 mL/min by employing a Mettler DSC-822 instrument (Mettler Toledo, Milan, Italy). The thermal characterization protocol involved a first heating cycle from 30 to 150 °C, a cooling cycle from 150 to 30 °C, and a second heating cycle from 30 to 250 °C, with heating/cooling rate of 10 °C/min. Glass transition temperature (T_g) was obtained at the inflection point in the heat flow vs temperature thermograms. Temperatures corresponding to the maximum of the exothermic (T_{exo}) and endothermic peaks (T_{endo}), as well as the endothermic peak area of the (ΔH_{ENDO}) were also acquired. Three sample replicates for each kind of scaffold were tested.

2.8. Scanning electron microscopy (SEM)

A JSM 5600LV SEM instrument (JEOL, Tokyo, Japan) was used to conduct a morphological analysis of the top surface and transversal cross-section, obtained through fracturing in liquid nitrogen, of the dry samples. After mounting the samples on an SEM stub, they were coated with platinum through sputtering. The samples were then viewed at varying magnifications, ranging from 200× to 8000×. Fiber diameter (d_f) and pore dimension (d_p) were measured on top-view micrographs (200× magnification) by means of ImageJ 1.43u software (National Institutes of Health, Bethesda, MD), taking over 20 measurements per specimen.

2.9. Cell culture

The mouse embryo fibroblast cell line Balb/3T3 clone A31 (American Type Culture Collection, ATCC CCL-163) was employed for hydrogels biological characterization. Cells were grown in Dulbecco's Modified Eagle's Medium (DMEM, Sigma-Aldrich, Milan, Italy) supplemented with 4 mM L-glutamine, 1 % penicillin:streptomycin solution (10000 U/mL:10 mg/mL), 10 % Calf serum, and antimycotic (37 °C, 5 % CO_2-enriched environment).

2.9.1. Cell seeding

Samples were inserted into a 24-well plate, sterilized with UV radiation for 10 min on each side, and then incubated for 30 min with a 70 % v/v EtOH aqueous solution. After that, the scaffolds were thoroughly washed with Dulbecco's phosphate buffer saline (DPBS), containing a 1 % penicillin/streptomycin solution. The samples were then incubated for 24 h at 37 °C, 5 % CO_2 after the solution had been replaced with complete culture medium. Following Cs-based scaffold cell seeding protocols optimized during previous studies on long term (≥2 weeks) cell culture experiments (Ma et al., 2001; Puppi et al., 2016), 3×10^4 cells were then seeded onto each scaffold in a 24 well plate and, after 30 min of incubation at 37 °C and 5 % CO_2, complete medium volume was adjusted to 500 μL, followed by incubation in a humidified atmosphere at 37 °C and 5 % CO_2.

2.9.2. Cell viability assay

Cell viability was evaluated on three samples of each type of scaffold cultured up to 14 days by means of the WST-1 cell proliferation reagent, based on mitochondrial enzyme-mediated conversion of a tetrazolium salt into formazan (soluble in the culture medium). Cell-seeded samples were incubated at 37 °C and 5 % CO_2 for 4 h with the WST-1 reagent, diluted 1:10 in cell culture medium. Absorbance measurements of formazan dye at 450 nm with a reference wavelength at 655 nm were carried out by means of a microplate reader (Biorad, Milan, Italy). Cells cultured on tissue culture polystyrene (TC-PS) were used as a control.

Cell viability was further assessed by Live/Dead assay. Samples were quickly washed 3 times with DPBS and incubated with Live/Dead stain (Thermo-Fisher Scientific, Waltham, USA) at a concentration of 2 μM calcein-AM and 4 μM ethidium homodimer-1 for 40 min at RT. The presence of live (green) and non-viable/dead (red) cells was assessed using a Nikon Eclipse TE2000 inverted microscope equipped with an EZ-C1 confocal laser (Nikon, Tokyo, Japan).

2.9.3. Cell morphology and scaffold colonization

Cell morphology and scaffold colonization 14 days after seeding were investigated by SEM. Samples were washed twice with DPBS, and the cells were then fixed through 1 h incubation with a 2 % glutaraldehyde solution in PBS. The samples were then washed with PBS 1× and treated for 1 min with sodium cacodylate (Sigma) 0.1 M, at pH 7.4. The specimens were then washed with six aqueous solutions (15 min each) containing increasing concentrations of EtOH from 10 to 100 % v/v. The samples were fixed on SEM stubs, platinum sputter coated, and then analyzed by SEM at different magnifications (200–8000×).

2.10. Statistical analysis

Experimental data are expressed as average ± standard deviation. One-way analysis of variance (ANOVA) and a Tukey test for post hoc analysis were employed to determine statistical differences ($p < 0.05$).

3. Results and discussion

3.1. Scaffold fabrication

PEC suspension preparation involved adding a given amount of Cs to a HA solution in dH_2O (1 % w/v). The addition of acetic acid (1 % v/v) to the obtained suspension caused Cs amine groups protonation and the subsequent PEC formation under vigorous magnetic stirring for some days. This gave the polyions sufficient time to spontaneously form electrostatic interactions between their opposite charges, responsible for PEC assembly.

Hydrogel fabrication was carried out by means of a CAWS process involving the extrusion of a HA/Cs PEC suspension through a translating needle, whose tip was immersed into an EtOH bath (Fig. 1). The computer-controlled motion of the needle and the deposition platform allowed the deposition of an extruded PEC filament with a predefined 0–90° pattern to fabricate a layered structure. Interlayer welding during this process is due to polymer chains diffusion at the interface between two fibers during the coagulation process. This allows the formation of a 3D cohesive hydrogel network with a macroporous structure (Chiellini et al., 2016).

Different experimental parameters that can affect PEC formation and its successful processing trough CAWS were investigated, such as the polymeric suspension composition and mixing conditions (Morelli, Puppi, & Chiellini, 2017). In particular, different HA/Cs weight ratios (80 to 20 %) were tested in order to optimize the printing process. When the HA/Cs ratio was either higher than 50 % or lower than 40 %, the formation of a continuous fiber was not achieved. However, a continuous fiber that could be deposited with a predefined pattern was obtained by employing a HA/Cs weight ratio of 50 or 40 %. Therefore, the hydrogel with a higher percentage of HA (HA/Cs 50 wt%) was selected as scaffold with optimized composition for subsequent post-printing treatment and characterization investigations. Optimized processing parameters allowing a consistent reproducibility of the scaffold shape and porous structure, included a flow rate (F) of 0.2 mL/h, a needle X-Y translational velocity (V_{dep}) of 540 mm/min, a needle inter-layer Z translation (d_Z) of 50 μm, and a needle tip-deposition surface initial distance (Z_0) of 2 mm. Scaffolds with two different thicknesses were developed, i.e., hydrogels composed of either 32 layers employed for chemical-physical, water-uptake, thermal, and morphological characterization, or 80 layers employed for in vitro cell culture experiments.

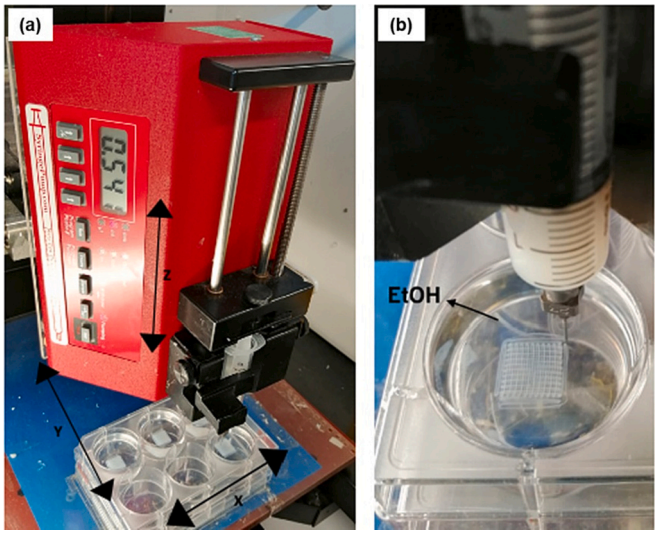

Fig. 1. AM equipment: representative picture of (a) CAWS apparatus, and (b) scaffold printing inside the EtOH coagulation bath.

As previously mentioned, various articles have been focused on HA/Cs porous hydrogels by employing different material processing techniques, e.g., wet-spinning (Yamane et al., 2005) and freeze-drying (Coimbra et al., 2011; Correia et al., 2011). In comparison with them, the described CAWS approach allows a better control over the morphology of 3D HA/Cs hydrogels in terms of external geometry and pores dimension, which is of fundamental importance for cell adhesion and colonization (Braccini et al., 2022). The application of AM to HA/Cs processing has been also recently explored. Maiz-Fernández et al. (Maiz-Fernández et al., 2021) investigated the printing properties, self-healing ability, and drug release kinetics of HA/Cs hydrogels. In that case, hydrogels were fabricated following a printing process on different surfaces (e.g., polystyrene) at room temperature, by alternating the deposition of a Cs solution and a HA solution. However, due to the diffusion of the solutions on the printing surface, which limited their printability, it was possible to obtain systems composed of only 4 layers. Suo et al. (Suo et al., 2022) developed 3D viscoelastic scaffolds based on aminated HA/Cs hydrogels loaded with graphene oxide and prepared using the combination of low-temperature 3D printing technology and freeze-drying. The here described CAWS approach has made it possible to directly print PECs of HA/Cs, without pre-printing chemical modification of the polysaccharides, inside a coagulation bath, as a means to avoid marked diffusion phenomena of the freshly printed fiber, thus allowing the fabrication of scaffolds composed of up to 80 layers. However, it should be pointed out that the developed hydrogels required a post-printing chemical cross-linking treatment, as described in the following section, in order to stabilize their structure in aqueous environment.

3.2. Post-processing treatment

Post-printing hydrogel chemical cross-linking through treatment with poly(methyl vinyl ether-*alt*-maleic acid) (PMVEMA) was investigated. PMVEMA and polymers derived therefrom are available on the market under the name Gantrez™. PMVEMA, known for its biocompatibility and low toxicity, is widely used in thickening and suspending agents, denture adhesives, as well as in adjuvants for drug delivery systems, hair care, transdermal patches, and mouthwashes (Dhiman et al., 2008; Goetz et al., 2010; Gómez et al., 2006; Gómez et al., 2007; Salas et al., 2008; Yoncheva et al., 2005). In addition, it has been recently used for tissue engineering scaffolds, as well as to cross-link freeze dried HA through esterification between polysaccharide hydroxyl groups and the PMVEMA carboxyl groups (Bucatariu et al., 2020; Larrañeta et al., 2018).

3.2.1. Optimization of temperature

Two post-processing treatment processes aimed at hydrogel cross-linking via transesterification between PMVEMA and the polysaccharide matrix were investigated in order to increase scaffold stability in a physiological environment (Fig. 2a). An involvement of the hydroxyl groups of Cs in the transesterification reaction should also be

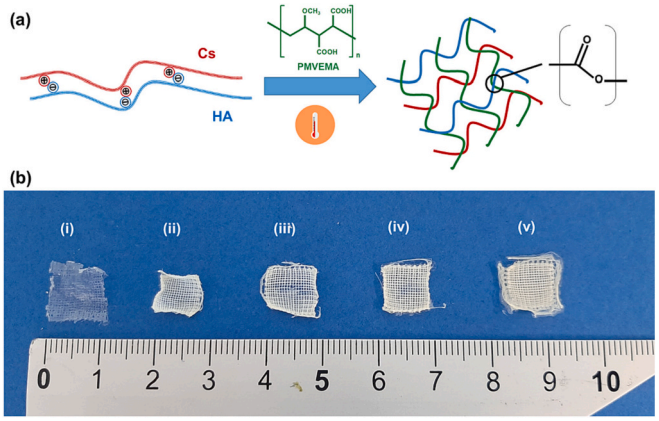

Fig. 2. (a) Proposed cross-linking mechanism through transesterification between the PMVEMA carboxyl groups and the polysaccharide hydroxyl groups by heat treatment, and (b) representative picture of HA/Cs scaffolds treated with different concentrations (w/v%) of PMVEMA: i) 0, ii) 1, iii) 2.5, iv) 5 and v) 7.5 %.

taken into account.

The developed post-printing treatments differ in time, mode, and temperature of incubation in a PVMEMA solution (5 % w/v), by keeping constant the time of thermal treatment (24 h) (Table 1). The first one (post-printing treatment at 80 °C) involved first scaffold incubation in an EtOH solution of PMVEMA for 5 h at RT, in order to allow cross-linker absorption, followed by sample removal from the solution and its treatment at 80 °C for 24 h, as previously proposed for freeze-dried HA samples (Larrañeta et al., 2018). In the second one (post-printing treatment at 65 °C) the scaffold was directly incubated in an EtOH solution of PMVEMA at 65 °C for 24 h to allow material cross-linking. This temperature was selected since it is lower than the normal boiling temperature of EtOH (78.3–78.8 °C). HA/Cs scaffolds not submitted to post-processing treatment and HA/Cs/PMVEMA scaffolds only incubated in a PMVEMA/EtOH solution for 5 h at RT, without subsequent thermal treatment, were used as controls. After post-printing treatments at high temperatures, both types of scaffolds were easy to handle; HA/Cs/PMVEMA 80 °C scaffold was distinguished from the other typology at a macroscopic level by a pale-yellow color and a more regular fibrous architecture.

3.2.2. Optimization of cross-linker concentration

The effect of the variation of the PMVEMA concentration in the cross-linking mixture was investigated in the case of post-printing treatment at 80 °C, since this protocol gave the best outcomes in terms of preservation and reproducibility of fibers alignment and scaffold shape, as well as a longer stability in aqueous solution (see Section 3.3.2). Scaffolds obtained after treatment with different concentrations of PMVEMA in the range 1 to 7.5 % w/v are shown in Fig. 2b.

3.3. Characterization

3.3.1. FTIR-ATR spectroscopy

FTIR-ATR spectroscopic analysis was carried out to investigate scaffold chemical composition and Cs/HA ionic interaction (Fig. 3).

Cs raw spectrum confirmed the presence of a band at 1644 cm^{-1} relevant to the carbonyl (C═O) stretching of *N*-acetyl groups (Dahmane et al., 2014; Fernandes Queiroz et al., 2015). Furthermore, it was possible to observe a band at 1540 cm^{-1} due to the overlapping of the N—H bending of the primary amine of the *N*-deacetylated groups and the bending of the secondary amide (N—H). Absorption bands characteristic of the polysaccharide structure were also detected, in particular at 1158 cm^{-1}, attributed to the asymmetric stretching of the C—O—C bridge, as well as at 1060 cm^{-1} and 1019 cm^{-1}, due to skeletal

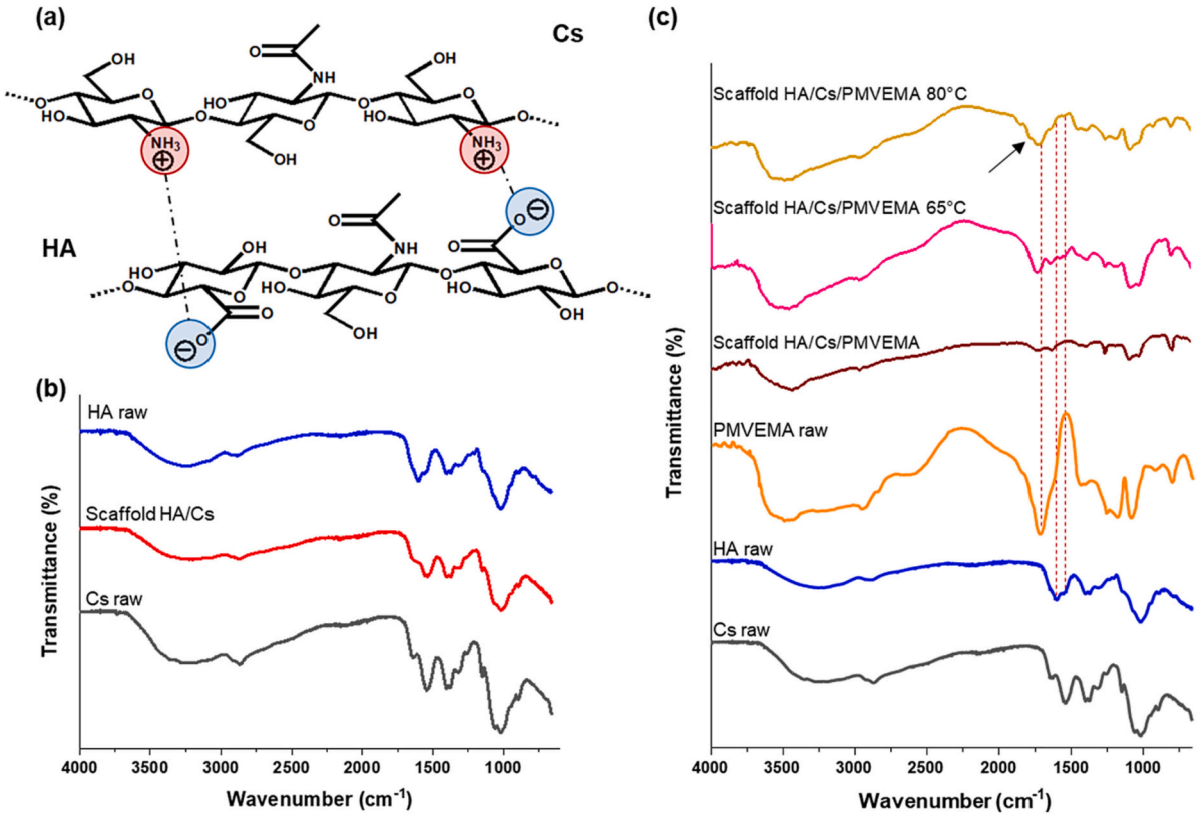

Fig. 3. (a) Schematic representation of hyaluronic acid (HA)/chitosan (Cs) polyelectrolyte complex (PEC) formation. FTIR-ATR spectra of: (b) Cs raw, HA raw and HA/Cs scaffold; (c) raw materials and HA/Cs/PMVEMA scaffolds submitted or not to heat treatments (arrow indicates the peak at 1780 cm^{-1}).

vibrations involving the C—O stretching. The characteristic band at 3342 cm^{-1} corresponding to the overlapping of the O—H and amino group (N—H_2) stretching vibrations was also observed (Fernandes Queiroz et al., 2015; Hamedi et al., 2019; Li et al., 2009). A broad absorption band at 3290 cm^{-1} due to OH and NH stretching vibrations was evident in the HA spectrum. A band at 2919 cm^{-1} is relevant to CH symmetrical and CH_2 asymmetrical stretching, while a band at 1610 cm^{-1} to C—O stretching of carboxylate anion. Ether bands, typical of carbohydrates, were observed at 1153 and 1020 cm^{-1} (Carneiro et al., 2016; Chen et al., 2019; Manju & Sreenivasan, 2011). PEC interaction resulted in a reduced intensity of the O—H and N—H stretching vibration peaks visible in scaffold HA/Cs spectrum. Moreover, the superposition of the bands relevant to the HA carboxylate groups and the Cs amine/amide groups resulted in a peak shift at 1557 cm^{-1}, as described in previous studies (Coimbra et al., 2011; Lewandowska et al., 2017).

Analysis of FTIR spectra of raw PMVEMA and scaffolds HA/Cs/PMVEMA either submitted (HA/Cs/PMVEMA 80 °C and HA/Cs/PMVEMA 65 °C) or not (HA/Cs/PMVEMA) to heat treatments was also carried out to ascertain cross-linking occurrence (Fig. 3c). In the post-printing treated scaffolds spectra it was possible to observe the characteristic peaks of raw PMVEMA: a band at about 2942 cm^{-1} relevant to the stretching of the C—H bond, a band at about 1700 cm^{-1} due to the stretching of the C═O group, and a band at 1078 cm^{-1} relevant to the symmetric stretching of the C—O bond. As already reported (Larrañeta et al., 2018), in the region between 1800 and 1500 cm^{-1} of the scaffold spectrum it is possible to observe a shift to higher wavenumbers of the bands related to the carbonyl peak of the carboxyl group of PMVEMA and the carbonyl peaks of the amide and carboxyl groups of HA, attributable to interactions between HA and PMVEMA chains. This shift could be explained with the more intimate interaction between the two macromolecular chains. Raw HA is characterized by non-covalent intermolecular interactions, mainly hydrogen bonds between carboxyl and hydroxyl groups in the polysaccharide chains. When PMVEMA and HA are combined, HA-HA interactions are less frequent due to the presence of PMVEMA between HA chains and its reaction with functional groups of the polysaccharide (Jia et al., 2015; Larrañeta et al., 2018).

In the carbonyl region shown in Fig. 3c, it is evident a broadening of the band of the HA/Cs/PMVEMA 65 °C and HA/Cs/PMVEMA 80 °C scaffolds compared to that of HA/Cs/PMVEMA scaffolds, due to the overlapping of the bands relevant to ester bond and those of the carbonyl group of carboxylic acids. Furthermore, for the HA/Cs/PMVEMA 80 °C scaffolds it is possible to observe a new peak at about 1780 cm^{-1}, correlated to reactions between free carboxyl groups of PMVEMA during post-printing treatment with the formation of anhydride groups.

3.3.2. *Water uptake (WU)*

The hydrogels were incubated in PBS 1× (pH = 7.4) at 37 °C to study their WU at predefined experimental time points until sample's breaking (Fig. 4). Different results were obtained depending on scaffold chemical

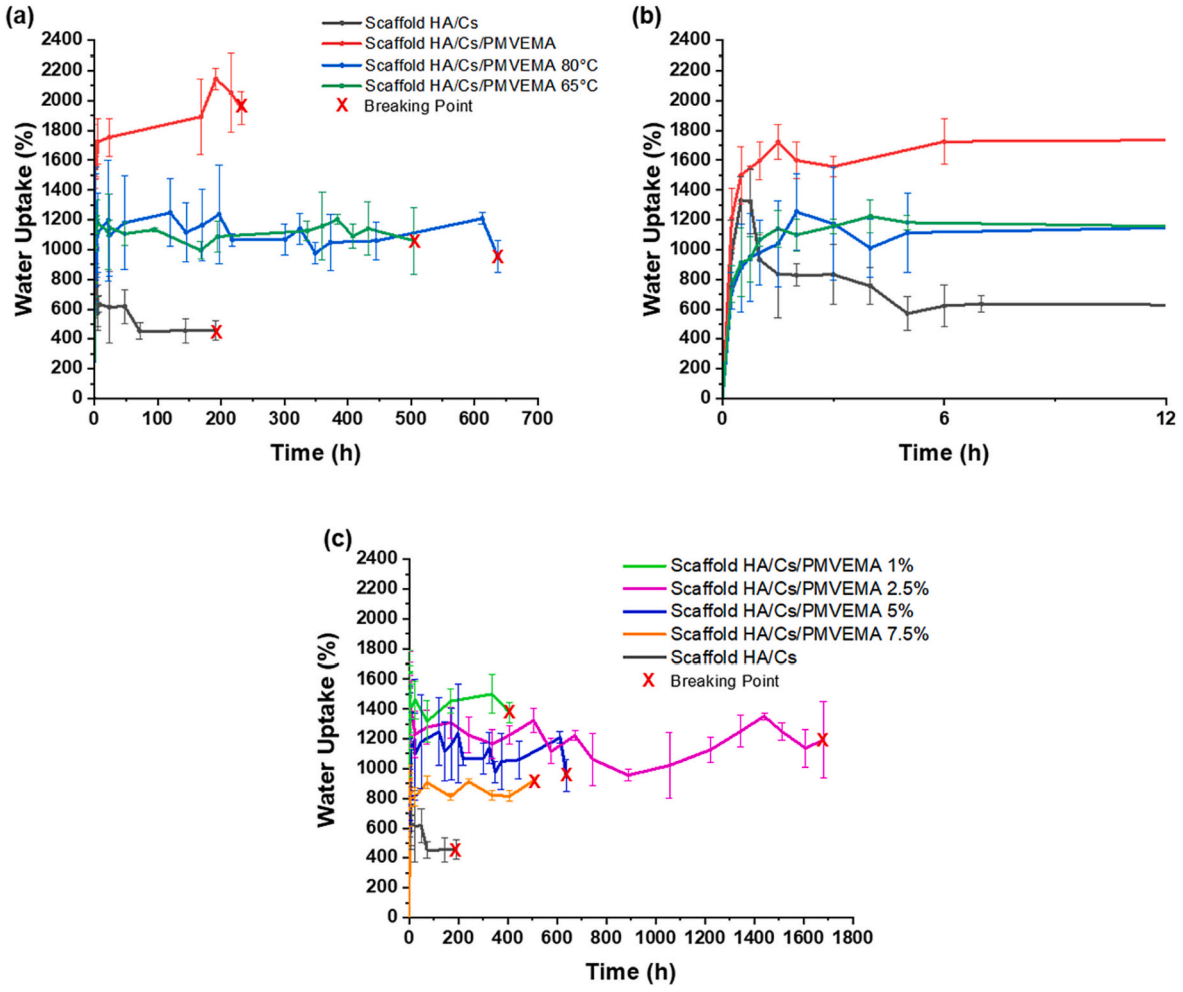

Fig. 4. Scaffold water uptake (WU) as a function of time (PBS 1×, 37 °C). Comparison of scaffolds based on the type of heat treatment: (a) up to sample breaking and (b) up to 12 h of analysis. (c) Comparison of scaffolds based on the different concentrations of PMVEMA. Data reported as mean (error bars representing ± standard deviation, n = 3).

composition and post-printing treatment. A first test was carried out on scaffolds treated by employing a 5 % w/v PMVEMA solution in EtOH. In this case, HA/Cs/PMVEMA, HA/Cs/PMVEMA 65 °C, and HA/Cs/PMVEMA 80 °C scaffolds reached a maximum WU value within 2 h of incubation, followed by a plateau at an equilibrium value that remained roughly stable during the whole assay (Fig. 4a, b). The HA/Cs scaffold instead reached a peak within the first 45 min of incubation followed by a progressive weight loss until breaking after 200 h. This phenomenon can be related to HA removal from the scaffold, because of its high solubility in aqueous environment (Dovedytis et al., 2020). For this reason, it is clear the necessity to cross-link the PEC in order not to lose HA in a physiological environment and compromise scaffold structural integrity.

The HA/Cs/PMVEMA 65 °C and HA/Cs/PMVEMA 80 °C scaffolds showed similar values of equilibrium WU (~1200 %), lower than that (~1600 %) of the scaffold which had not undergone heat treatment (HA/Cs/PMVEMA). In agreement with what was shown by FT-IR spectroscopy, this result suggests a higher degree of cross-linking given by ester bonds between HA and PMVEMA in the case of heat treatment. In addition, while HA/Cs/PMVEMA scaffold broke after 240 h, HA/Cs/PMVEMA 65 °C and HA/Cs/PMVEMA 80 °C scaffolds were stable for a period longer than 500 h, resulting suitable for long incubation times in physiological conditions. As shown in Fig. 4c, WU of scaffolds treated at 80 °C with different concentrations of PMVEMA in the range 1–7.5 % w/v was also evaluated. PBS retention ability of the scaffold increased by decreasing cross-linker concentration, in agreement with the results of other studies (Gierszewska & Ostrowska-Czubenko, 2016). Indeed, among the various aspects potentially influencing hydrogel WU ability (e.g., ionization of the functional groups and ionic strength of the medium) polymeric network cross-linking degree has been often shown to have a significant role. Breaking time was also markedly affected by PMVEMA concentration, ranging from 438 h for 1 % w/v to 1736 h for 2.5 % w/v.

HA/Cs/PMVEMA scaffolds treated with a 5 % w/v concentration were selected for further characterization tests since they allow the best compromise in terms of handling and stability in physiological conditions. Indeed, even if they showed markedly longer breaking time, scaffolds treated with a 2.5 % w/v PMVEMA solution became warped once incubated in PBS.

Summarizing, PMVEMA cross-linking was demonstrated to be a suitable means for HA/Cs hydrogels stabilization in aqueous environment by avoiding fast HA solubilization. Despite that, a class of enzymes, known as esterases, can hydrolyze within the human body the ester bond between PMVEMA and the HA/Cs scaffold. These enzymes combine a molecule of water or a hydroxide ion to hydrolyze the ester bond and produce a carboxylic acid and an alcohol (Laizure et al., 2013). Moreover, Cs is primarily broken down in vivo through an enzymatic hydrolytic degradation by lysozyme, involving cleavage of the glycosidic linkages between the polysaccharide units with the formation of oligosaccharide and saccharide byproducts, which are either incorporated into proteoglycans or metabolized by the body (Jennings, 2017). HA is instead mainly degraded by hyaluronidases, a class of enzymes that break down HA into monosaccharides by splitting the β-1,4 glycosidic bonds (Jung, 2020).

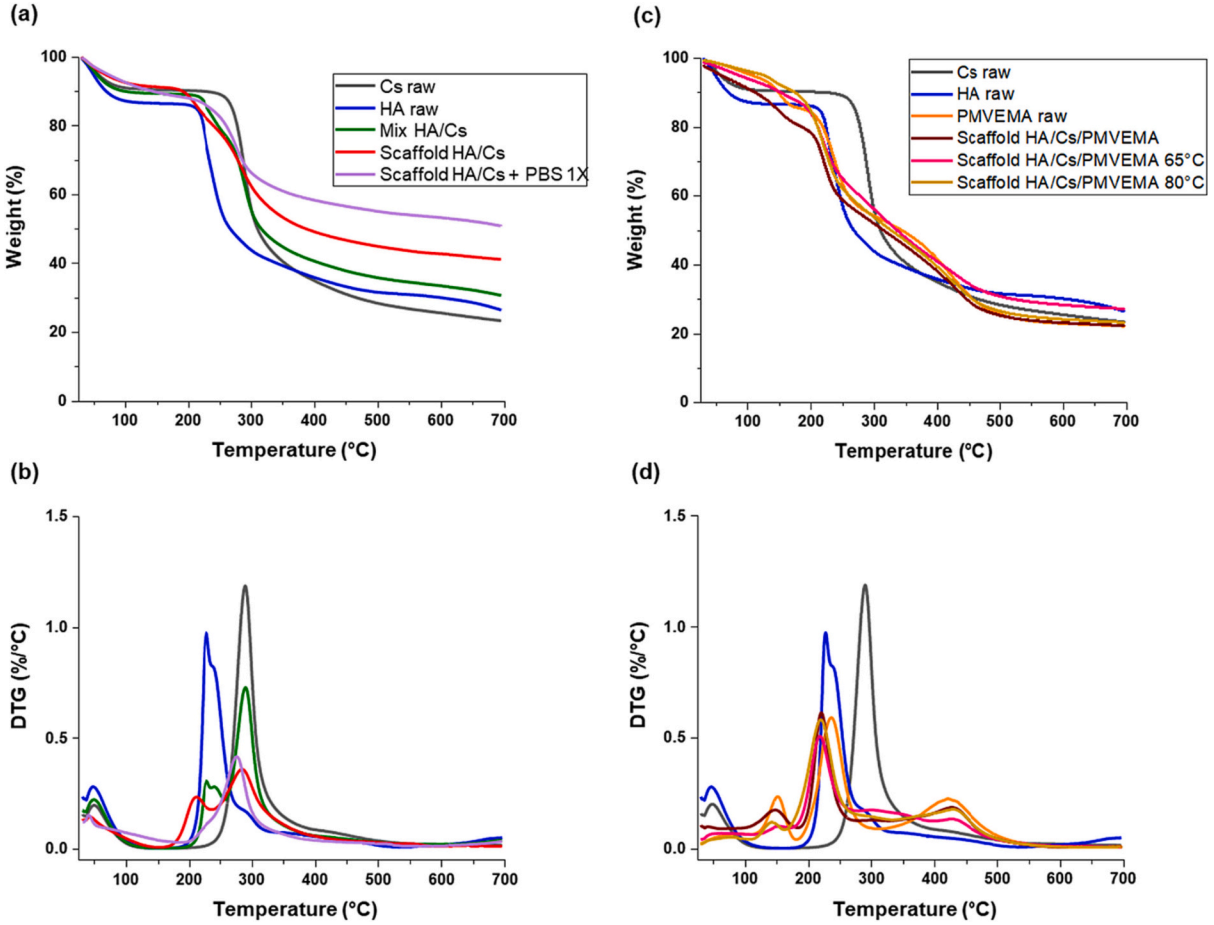

Fig. 5. Representative TGA thermograms relevant to weight loss and derivative of weight (DTG) vs. temperature of (a, b) raw polymers, HA/Cs physical mixture (Mix HA/Cs), HA/Cs scaffold and HA/Cs scaffold after incubation in PBS 1× (37 °C), and (c, d) raw polymers and HA/Cs/PMVEMA scaffolds with and without heat treatment.

3.3.3. Thermogravimetric analysis (TGA)

TGA was employed to analyze the developed scaffolds, raw Cs and HA, as well as a CS/HA physical mixture (Fig. 5a, b).

Weight derivative thermograms of all samples were characterized by a first peak between 43 and 72 °C related to the presence of moisture. In addition, raw polymers weight derivative curves were characterized by a peak centered at around 226 °C (T_{max2}) or 296 °C (T_{max4}) relevant to HA or Cs, respectively (Table 2). Polysaccharides thermal degradation is the result of dehydration of the saccharide rings, depolymerization, and decomposition of the saccharidic repeating units (Cárdenas-Triviño et al., 2017; Piras et al., 2014). HA/Cs physical mixture and HA/Cs scaffold thermograms were characterized by two thermal degradation events corresponding to those of the raw materials. In particular, the derivative curves showed a T_{max2} between 210 and 227 °C and a T_{max4} between 285 and 289 °C (Table 2). Scaffold HA/Cs showed significantly lower T_{max2} and T_{max4} than raw polymers. As hypothesized in previous articles focused on HA/Cs and other CS-based PECs (Boobphahom et al., 2020; Finnberg et al., 2017), shifts of derivative peaks occur when the two polyions are effectively complexed and not simply physically-blended. Furthermore, the thermograms of the HA/Cs scaffold after PBS 1× incubation (scaffold HA/Cs + PBS 1×) showed only the peak related to the presence of Cs (276 ± 1 °C), confirming HA loosing due to solubilization.

HA can be modified to improve its stability and tailor its in vivo degradation profile, in order to favor cell adhesion and subsequent proliferation (Tiwari & Bahadur, 2019). The relatively simple polysaccharide structure can be easily modified through reaction with its hydroxyl (Andrade del Olmo et al., 2021; P et al., 2021) and carboxyl groups (Kwon et al., 2019; Turner et al., 2004), as well as upon deacetylation of the acetamide groups and subsequent modification of the obtained amine groups (Tiwari & Bahadur, 2019). The cross-linking procedures described in this work involve the use of PMVEMA, a polymer used for the formation of biomedical hydrogels thanks to its demonstrated cytocompatibility (Demir et al., 2017; T. Zhang et al., 2013).

In the thermogram of raw PMVEMA (Fig. 5c, d) it is possible to note three weight loss events, associated to three peaks at about 150 (T_{max1}), 235 (T_{max3}) and 423 °C (T_{max5}) (Table 2) and due respectively to dehydration of acid groups, as well as decarboxylation and other degradation reactions of the macromolecular chain (Nair et al., 2014).

In the thermograms of scaffolds treated with PMVEMA (5 % w/v), with or without a thermal treatment, i.e., HA/Cs/PMVEMA, HA/Cs/PMVEMA 65 °C, and HA/Cs/PMVEMA 80 °C, it is possible to observe the peaks related to PMVEMA weight losses. Moreover, the degradation peaks of raw PMVEMA, raw HA, and raw Cs overlap in the temperature range 200–350 °C. This aspect limits the univocal identification of degradation peaks related to HA and Cs in PMVEMA-treated samples.

Table 2
T_{max} data relevant to raw materials, HA/Cs physical mixture and scaffolds, obtained from TGA analysis.

Sample	T_{max1}	T_{max2}	T_{max3}	T_{max4}	T_{max5}
Cs raw				296 ± 1[a]	
HA raw		226 ± 1[*,#,##]			
PMVEMA raw	150 ± 1[b]		235 ± 1[c]		423 ± 3[§,§§]
Mix HA/Cs		227 ± 1[**]		289 ± 1[a]	
Scaffold HA/Cs		210 ± 1[*,**]		285 ± 1[a]	
Scaffold HA/Cs + PBS 1×				276 ± 1[a]	
Scaffold HA/Cs/PMVEMA	147 ± 1[b,○]		219 ± 1[c]		428 ± 2
Scaffold HA/Cs/PMVEMA 65 °C	151 ± 2[○,○○]		216 ± 1[c,#]		430 ± 2[§]
Scaffold HA/Cs/PMVEMA 80 °C	141 ± 1[b,○○]		218 ± 2[c,##]		430 ± 1[§§]

Values are reported as mean ± standard deviation (n = 3). Data marked with the same symbol are statistically different from each other ($p < 0.05$).

3.3.4. Evolved gas analysis - mass spectrometry (EGA-MS)

EGA-MS was carried out to study thermal decomposition and stability of raw materials, physical mixtures, HA/Cs/PMVEMA 80 °C and HA/Cs/PMVEMA scaffolds. The total ion thermograms (TITs, Fig. 6a–c) relevant to volatile products in the 50–700 °C temperature range showed Cs raw thermal degradation between 226 °C (7 min) and 675 °C (25 min), HA raw degradation between 230 °C (7 min) and 561 °C (20 min), and a PMVEMA raw degradation between 226 °C (7 min) and 750 °C (28 min). Evolved gases maxima were at 333 °C and 454 °C for Cs raw, 273 °C for HA raw, and 463 °C for PMVEMA raw. A shoulder after 12 min (360 °C) and 8 min (261 °C) for HA and PMVEMA raw, respectively, was observed. The thermograms of both binary and ternary physical mixtures were a perfect overlap of those of the raw materials. On the contrary, scaffolds thermograms (Fig. 6c) showed a maximum of evolved gas at a higher temperature (468 °C) with a shoulder after 8 min (250 °C). Moreover, the thermogram of thermally-cross-linked scaffold (green line) presented another shoulder between 300 and 375 °C (10–13 min). These differences could be the result of inter- and intra-molecular interactions between the different scaffold components, requiring different amounts of thermal energy to break down and release the same degradation products of raw materials, as the scaffolds have a greater thermal stability. Figs. 6d–f show the extract ion thermograms (EIT) of main products of raw Cs released during EGA-MS analysis: fragment ion at *m/z* 59 corresponding to acetamide (*m/z* **43**, 59), fragment ion at *m/z* 67 corresponding to pyrrole (*m/z* 39, 52, **67**) and *m/z* 114 from methyl *N*-acetyl-d-glucosamide (*m/z* 43, **59**, 72, 101, 114); HA: fragment ion at *m/z* 59 from acetamide, *m/z* 125 from 3-amino-2-isopropyl-5-methyl-2H-pyrazole (*m/z* 43, 55, **83**, 110, 125); and PMVEMA: fragment ion at *m/z* 67 from 2-methyl-2-cyclopenten-1-one (*m/z* 39, 53, **67**, 96), *m/z* 77 corresponding to p-xylene (*m/z* 51, 77, **91**, 106) and *m/z* 91 to toluene (*m/z* 51, 65, **91**, 92).

The extract ion thermograms (EITs) of relevant fragment ions corresponding to gaseous products released during EGA-MS analysis of a physical mixture of polymers (Mix HA/CS/PMVEMA) and scaffolds (Scaffold HA/CS/PMVEMA and Scaffold HA/CS/PMVEMA 80 °C) are shown in Fig. 7. It was therefore possible to monitor the thermal decomposition behavior of polymers while involved or not (pure physical mixture) in cross-linking and scaffold formation. The distribution of the evolved gases with the fragment ions at *m/z* 59, 67, 114 and 125, corresponding to acetamide from Cs and HA, pyrrole from Cs, methyl *N*-acetyl-D-glucosamide from Cs and 3-amino-2-isopropyl-5-methyl-2H-pyrazole from HA, was completely different for the mixture (green line) and for the scaffold (red and black lines). This confirmed the presence of inter- and intra-polymer interactions between scaffold components versus their absence in the mixture. Despite the minimum difference in the shape of EIT of *m/z* at 77 and 91 between the mixture and scaffolds, a shift of the maximum at higher temperatures in case of scaffolds is detected, indicating their greater resistance to degradation, thus the presence of inter- and intra-polymeric interactions.

It was also possible to evaluate the post-printing treatment carried out on the scaffold treated at 80 °C by monitoring fragment ion at *m/z* 125. Scaffold without treatment (black line) forms 3 maxima which correspond to the maxima present in the mixture (green line) and in the cross-linked product after treatment (red line), highlighting that the untreated scaffold is an intermediate product, possibly containing the reactants still in a non-reticulated form.

3.3.5. Differential scanning calorimetry (DSC)

The fabricated scaffolds, as well as relevant raw polymers and their physical mixture, were characterized by DSC. During the first heating cycle only a broad endothermic peak relevant to evaporation of

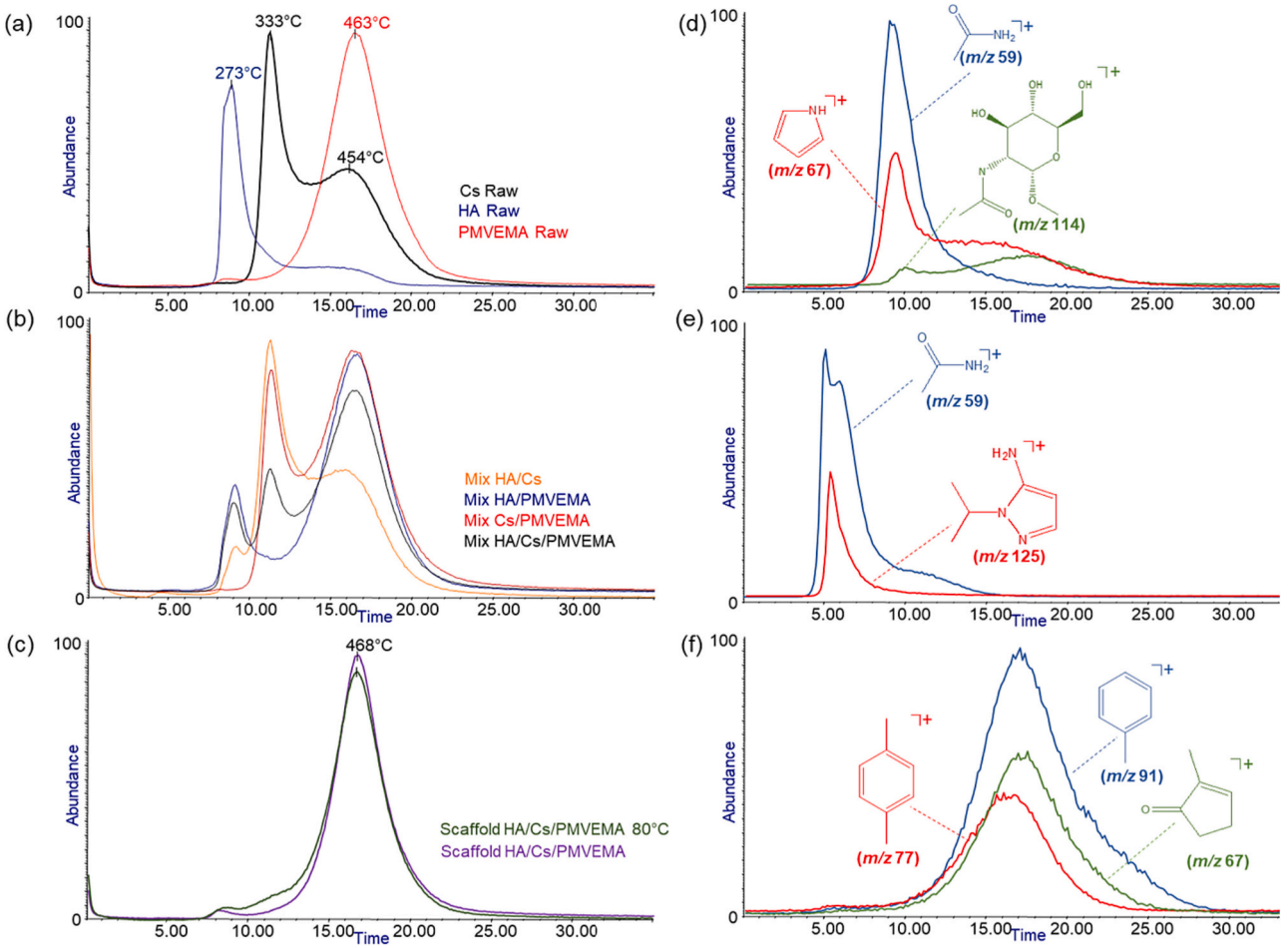

Fig. 6. Total ion thermograms (TITs) of (a) raw polymers, (b) their physical mixtures, and (c) scaffolds; extract ion thermograms (EITs) of evolved gas during thermal degradation of (d) Cs, (e) HA and (f) PMVEMA raw materials.

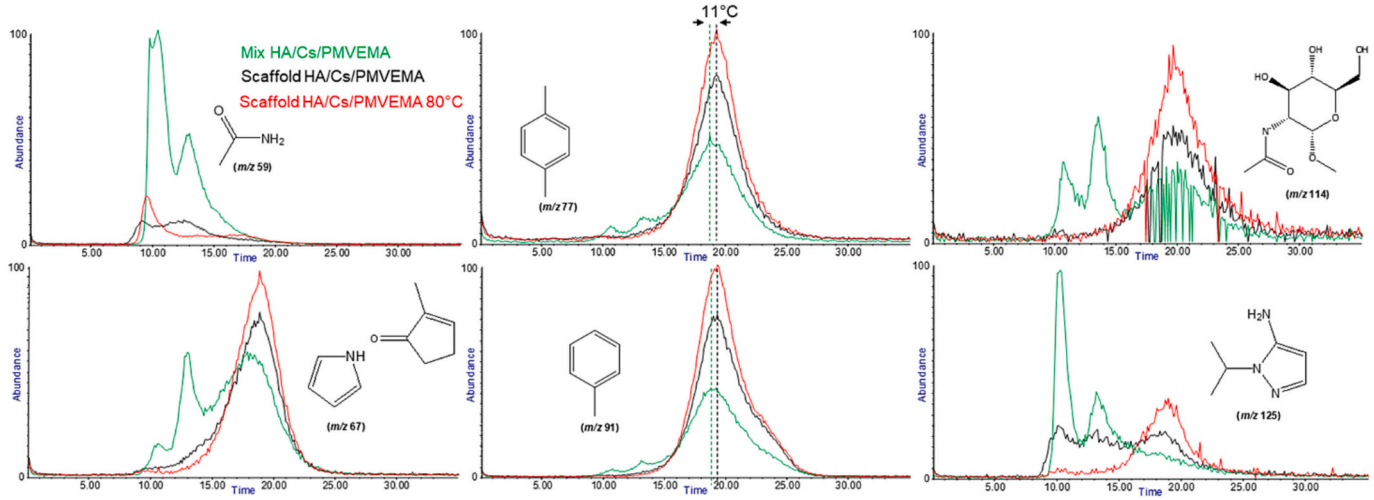

Fig. 7. Extract ion thermograms (EITs) of evolved gas during thermal degradation of the physical mixture mix HA/Cs/PMVEMA, HA/Cs/PMVEMA scaffold, and HA/Cs/PMVEMA 80 °C scaffold.

absorbed water molecules was evident. The analysis of the second heating cycle thermograms highlighted a glass transition, as well as exothermic and endothermic peaks. In particular, raw Cs had a glass transition temperature (T_g) of around 112 °C (Fig. 8a and Table 3), corroborating what reported by previous articles (Nair et al., 2014). The raw HA thermogram showed a T_g of around 119 °C and an exothermic peak centered at around 236 °C correlated to polymer degradation (Han et al., 2012; Larrañeta et al., 2018). In the HA/Cs physical mixture (Mix HA/Cs) thermogram it was possible to identify a T_g and the exothermic peak characteristic of raw HA. In the thermogram of HA/Cs scaffold it

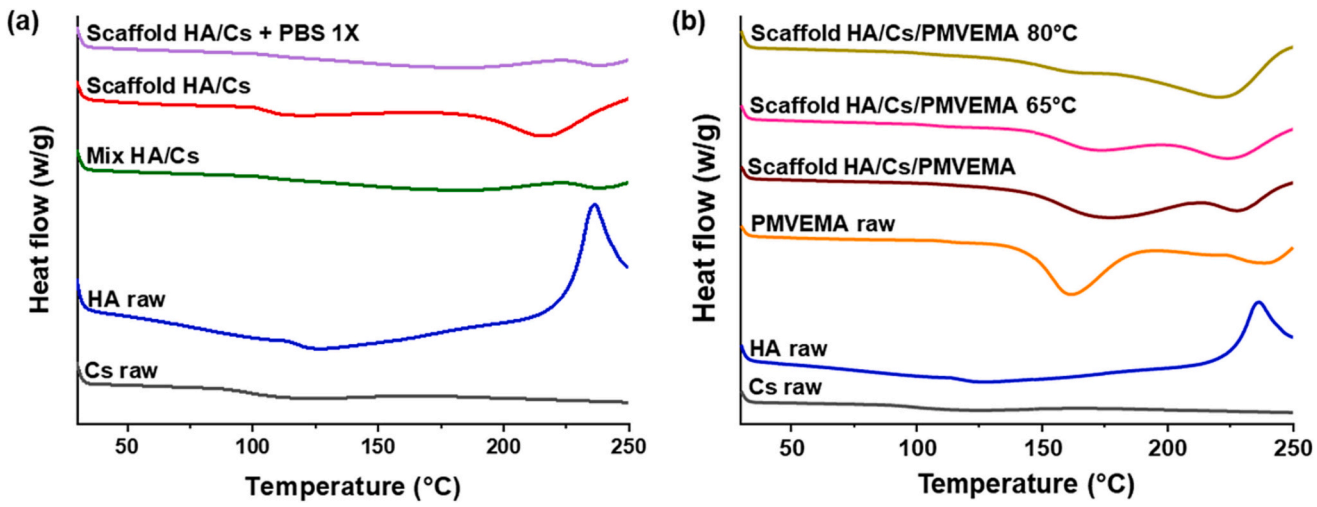

Fig. 8. DSC thermograms relevant to the second heating of raw Cs, raw HA, (a) HA/Cs physical mixture, HA/Cs scaffold and HA/Cs scaffold after incubation in PBS 1× and (b) raw PMVEMA, HA/Cs/PMVEMA scaffolds (PMVEMA 5 % w/v) submitted or not to heat treatments (Exo up for all thermograms).

Table 3
Data relevant to T_g and enthalpy peaks obtained from DSC analyses.

Sample	T_g (°C)	T_{exo} (°C)	T_{endo1} (°C)	T_{endo2} (°C)	ΔH_{ENDO1} (J/g)$^{+}$	ΔH_{ENDO2} (J/g)
Cs raw	112 ± 21					
HA raw	119 ± 6	236 ± 1				
PMVEMA raw	118 ± 11		161 ± 1*,**	240 ± 1$^{\circ,\circ\circ}$	117.8 ± 6.2	36 ± 1$^{\hat{}}$
Mix HA/Cs	104 ± 6	236 ± 1				
Scaffold HA/Cs	104 ± 1		216 ± 1			
Scaffold HA/Cs + PBS 1×	104 ± 2	224 ± 1				
Scaffold HA/Cs/PMVEMA	119 ± 5		176 ± 1*	227 ± 1$^{a,\circ\circ}$	91.1 ± 5.8	26 ± 4$^{\#}$
Scaffold HA/Cs/PMVEMA 65 °C	114 ± 7		177 ± 3**	222 ± 1^{a}	29.6 ± 3.3	54 ± 6$^{\hat{},\#}$
Scaffold HA/Cs/PMVEMA 80 °C	114 ± 12		170 ± 9	221 ± 1$^{\circ,\circ\circ}$	8.7 ± 0.9	135 ± 2$^{\hat{},\#}$

Values are reported as mean ± standard deviation (n = 3).
Data marked with the same symbol are statistically different ($p < 0.05$).
$^{+}$ All values relevant to this parameter (ΔH_{ENDO1}) are statistically different ($p < 0.05$).

was possible to note a T_g centered at around 104 °C and an endothermic peak at 216 °C. An endothermic peak at T > 200 °C before thermal degradation was already described during previous studies involving Cs-based PEC characterization and generically ascribed to a phase transition occurring in the polymeric network (Martins et al., 2011; Polexe & Delair, 2013). However, the thermogram of the scaffold submitted to PBS incubation (scaffold HA/Cs + PBS1×) did not present this endothermic peak (Fig. 8a). This evidence can be related to the neutralization of Cs amine groups upon buffer incubation, resulting in Cs-HA intermolecular interactions similar to those occurring in the physical mixture (Mix HA/Cs), whose thermogram did not display any endothermic peak.

The thermogram related to raw PMVEMA showed two endothermic peaks centered at around 161 and 240 °C (Fig. 8b and Table 3). In the thermograms relevant to HA/Cs/PMVEMA scaffolds submitted or not to heat treatments, these two endothermic peaks significantly shifted to around 175 and 225 °C, respectively.

The two endothermic peaks observed in thermograms of PMVEMA-containing samples were related to reactions occurring during DSC analysis: a first one, more intense, attributable to the formation of anhydrides through reaction between free carboxyl groups, and the second one to the formation of an ester bond through reaction between PMVEMA carboxyl groups and hydroxyl groups of HA or Cs (Larrañeta et al., 2018). Compared to HA/Cs/PMVEMA scaffold not submitted to heath treatment, the HA/Cs/PMVEMA 65 °C and 80 °C scaffolds showed a smaller area of the first peak (ΔH_{ENDO1}) and a larger area of the second endothermic peak (ΔH_{ENDO2}) relevant to ester bond formation (Table 3). This could be due to post-printing macromolecules cross-linking which engaged the carboxyl groups of PMVEMA and the hydroxyl groups of the polysaccharide chains to form ester bonds. As a consequence, a smaller number of carboxyl groups were available for anhydride linkage formation in samples with a higher degree of cross-linking (HA/Cs/PMVEMA 65 °C and 80 °C), and the energy to carry on with transesterification was higher (Larrañeta et al., 2018).

3.3.6. *Scanning electron microscopy (SEM)*

SEM analysis of the top view (Fig. 9a) and transversal cross-section (Fig. 9b) of hydrogels not submitted to post-processing treatment (Scaffold HA/Cs) and thermally cross-linked (HA/Cs/PMVEMA 65 °C and 80 °C) were acquired to analyze the morphology of their 3D porous structure, as well as to measure their macropores (d_p) and fibers dimensions (d_f) (Table 4).

Top view micrographs of thermally cross-linked scaffolds showed aligned polymeric fibers (average diameter of 38–57 μm), forming a diffuse and interconnected porosity (average pore size of 327–452 μm). The HA/Cs scaffolds not submitted to post-processing treatment did not present a defined porous structure, while in the thermally cross-linked scaffolds it was possible to notice some pore occlusions, that could be due to the presence of an excess of PMVEMA. In the cross-section micrographs, it was possible to observe a layered porous structure for the HA/Cs/PMVEMA 80 °C scaffold, while in the case of HA/Cs/PMVEMA 65 °C scaffold a partial fusion between fibers of consecutive layers with consequent limited porosity was highlighted. Scaffold HA/Cs cross-section micrographs were not taken due to the impossibility of obtaining a sample cross-section through fracture in liquid nitrogen.

A large body of literature has highlighted that one of the main shortcomings of 3D printing of hydrogels made of natural polymers is related to a limited porosity in the direction of printing (Z axis) along the scaffold thickness, as observed in cross-section micrographs (Fig. 9b), due to a low rigidity of the material which is in a hydrated state (Li et al., 2018). This low control over scaffold morphology can in turn result in a limited control over hydrogel properties. Fibers misalignment and

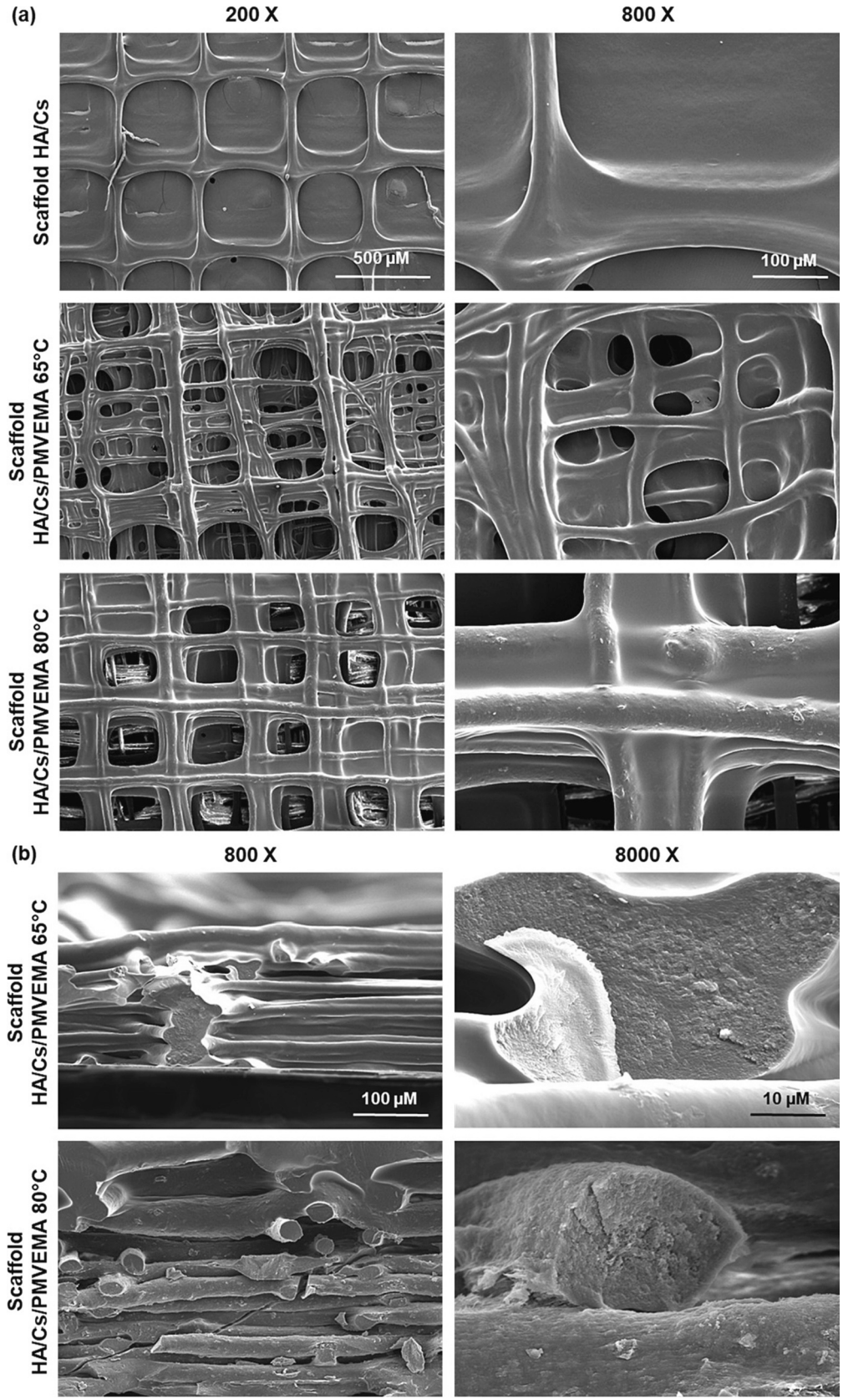

Fig. 9. Representative SEM micrographs relevant to (a) top view and (b) transversal cross-section of the developed scaffolds subjected to different post-printing treatment (dry state, magnifications 200×, 800×, and 8000×).

Table 4
Data obtained from SEM micrographs related to pore dimension (d_p) and fiber diameter (d_f).

Sample	d_p	d_f
Scaffold HA/Cs	426 ± 39*	43 ± 11°
Scaffold HA/Cs/PMVEMA 65 °C	452 ± 100**	38 ± 12°°
Scaffold HA/Cs/PMVEMA 80 °C	327 ± 20* **	57 ± 13° °°

Values are reported as mean ± standard deviation (n = 25).
Data marked with the same symbol are statistically different from each other ($p < 0.05$).

distortion were also evident in some top view micrographs (Fig. 9a), raising concerns about the reproducibility of hydrogel properties depending on scaffold macrostructure (e.g., water uptake and cell interactions). However, it should be considered that the dehydration treatment and platinum sputtering required to characterize the samples by SEM, as well as the subsequent analysis under vacuum, are critical steps markedly affecting the morphology of hydrogel fibrous structure. For this reason, the morphology of the scaffolds in the hydrated state can be markedly different from that observed in the recorded SEM micrographs shown in Fig. 9. In any case, all the characterization tests of this study aimed at collecting quantitative data were carried out on three different sample replicates for each kind of hydrogel, in order to statistically evaluate the differences between properties of different kinds of scaffold, taking into account sample morphology variability.

3.3.7. Biocompatibility

Preliminary in vitro cell culture experiments were carried out by employing the murine embryo fibroblast cell line Balb/3T3 clone A31 grown on non cross-linked HA/Cs scaffold, as well as on HA/Cs/PMVEMA 80 °C scaffold. The latter was selected as a representative thermally cross-linked scaffold since it was characterized by a more defined layered macroporous structure and a longer stability in aqueous environment in comparison to the other investigated hydrogel submitted to cross-linking. Newly developed medical devices must be tested for their biocompatibility as specified by the relevant international standard series ("ISO 10993-5:2009"). In particular, test by direct contact employing this cell line in combination with an assay for quantitative measurements of cell viability is recommended by the aforementioned standard. In this study, cell metabolic activity, directly related to cell viability, was investigated by means of WST-1 assay at day 1, 5, 9, and 14 after cell seeding on scaffolds HA/Cs and HA/Cs/PMVEMA 80 °C, as well as on tissue culture polystyrene (TC-PS) wells, used as a 2D control. Scaffolds composed of 80 layers were employed since they offered a higher surface area and could be more easily handled during cell culture experiments in comparison to the other developed scaffold type (32 layers).

A general absorbance increase over time was observed for all types of samples (Fig. 10a). In particular, a significant cell viability increase was measured in the case of HA/Cs scaffold at day 14 and for HA/Cs/PMVEMA 80 °C scaffold at day 9. In addition, the cross-linked scaffold showed a cell viability significantly higher than HA/Cs scaffold at all time points. This could be at least in part related to the stratified porous architecture of the cross-linked hydrogel (Fig. 9b) which allowed the cells to arrange and proliferate on multiple levels, as well as a better transport of nutrients and metabolic waste products, better mimicking the cellular environment in vivo (Rivero et al., 2020). Cells cultured on TC-PS were characterized at all time points by a higher viability than those grown on scaffolds, probably due to the well surface chemistry optimized for cell colonization. Cells grown onto a TC-PS surface, not subjected to any type of treatment, are indeed typically used as an internal control of the experiment to verify the quality of the analysis performed.

Analysis of Live/Dead micrographs (Fig. 10b) supported the results achieved by means of the quantitative WST-1 assay. In general, an increasing number of cells from day 1 to day 14 of culture was detected for the two types of scaffold investigated. HA/Cs/PMVEMA 80 °C scaffolds supported the colonization by a higher number of fully viable cells (in green) at all time points. Starting from day 9 of culture, cells were able to uniformly cover also the surface of HA/Cs scaffold fibers. However, in the latter case, a large number of dead cells (in red) and fibroblasts organized in cell clusters or ordered globular structures (spheroids) were detected (Fig. 10c). These phenomena could be related to the material surface chemistry, since it is well known that cells growing on highly hydrophilic surfaces are more susceptible to apoptosis (Brodbeck et al., 2001; Brodbeck et al., 2002). Furthermore, one of the most effective techniques for obtaining cellular spheroids involves the use of ultra-low attachment microplates, characterized by a covalently bound hydrophilic hydrogel (Braccini et al., 2022). It could be therefore speculated that, although its fast solubilization, a significant amount of residual HA combined in the hydrogel matrix is at the basis of the observed cell behavior. Indeed, HA hydrophilicity is often seen as a drawback causing low cell attachment and spreading (Yamanlar et al., 2011).

SEM micrographs of cells fixed on HA/Cs and HA/Cs/PMVEMA 80 °C scaffolds after 14 days of culture are shown in Fig. 11. Cells completely covered the fiber surface in both kinds of scaffold. In the case of HA/Cs/PMVEMA 80 °C scaffold, cells showed a stretched and flat morphology, while a high number of cells with a rounded morphology, a sign of poor adaptation and adhesion to the polymer substrate (Osório et al., 2021), was observed in HA/Cs sample, corroborating the results achieved by means of Live/Dead assay.

4. Conclusion

This research activity demonstrated that the CAWS technique can be effectively employed to fabricate HA/Cs PEC scaffolds with predefined shape, size, and 3D porous architecture. A noteworthy advantage of the developed fabrication approach is that Cs/HA scaffolds composed of tens of overlapped layers can be fabricated, thanks to an advanced control over the deposited filament morphology achieved through coagulation in a non-solvent. Indeed, previous articles on the application of AM to this kind of Cs/HA PEC resulted in the fabrication of scaffolds composed of few layers, or involved Cs chemical modification to obtain thicker samples. However, HA fast solubilization upon scaffold incubation in aqueous medium, as demonstrated by TGA, DSC, and water uptake analysis, required the optimization of a cross-linking strategy for the hydrogels developed in this study. Two different protocols based on PMVEMA as chemical cross-linker were developed and successfully applied to stabilize HA/Cs scaffolds in a physiological environment. Furthermore, the use of an optimized cross-linking treatment allowed fabricating a 3D structure with interconnected porosity along its thickness. In vitro cell culture investigations demonstrated the ability of these scaffolds to support murine fibroblast cell growth for 14 days, with increased cell viability levels in the case of PMVEMA cross-linked scaffolds.

Taken together, the results achieved in this study hold great potential of significantly impacting the current research trend on novel biocompatible materials for AM, complying with the concept of sustainable development by using modern key technologies. A natural progression of this work is the investigation of the developed scaffolds for long-term in vitro modelling of health or pathological tissues, to further validate the developed experimental fabrication protocol. For instance, Cs and HA have been previously proposed for cartilage tissue engineering thanks to their compatibility with chondrocytes and suitable mechanical properties for this application (Muzzarelli et al., 2012). In addition, Cs-based PECs are also good candidates for in vitro tumor modelling (Chiellini et al., 2016) and the investigation of the developed 3D printed HA/Cs hydrogels for cancer cell growth will be the object of future studies.

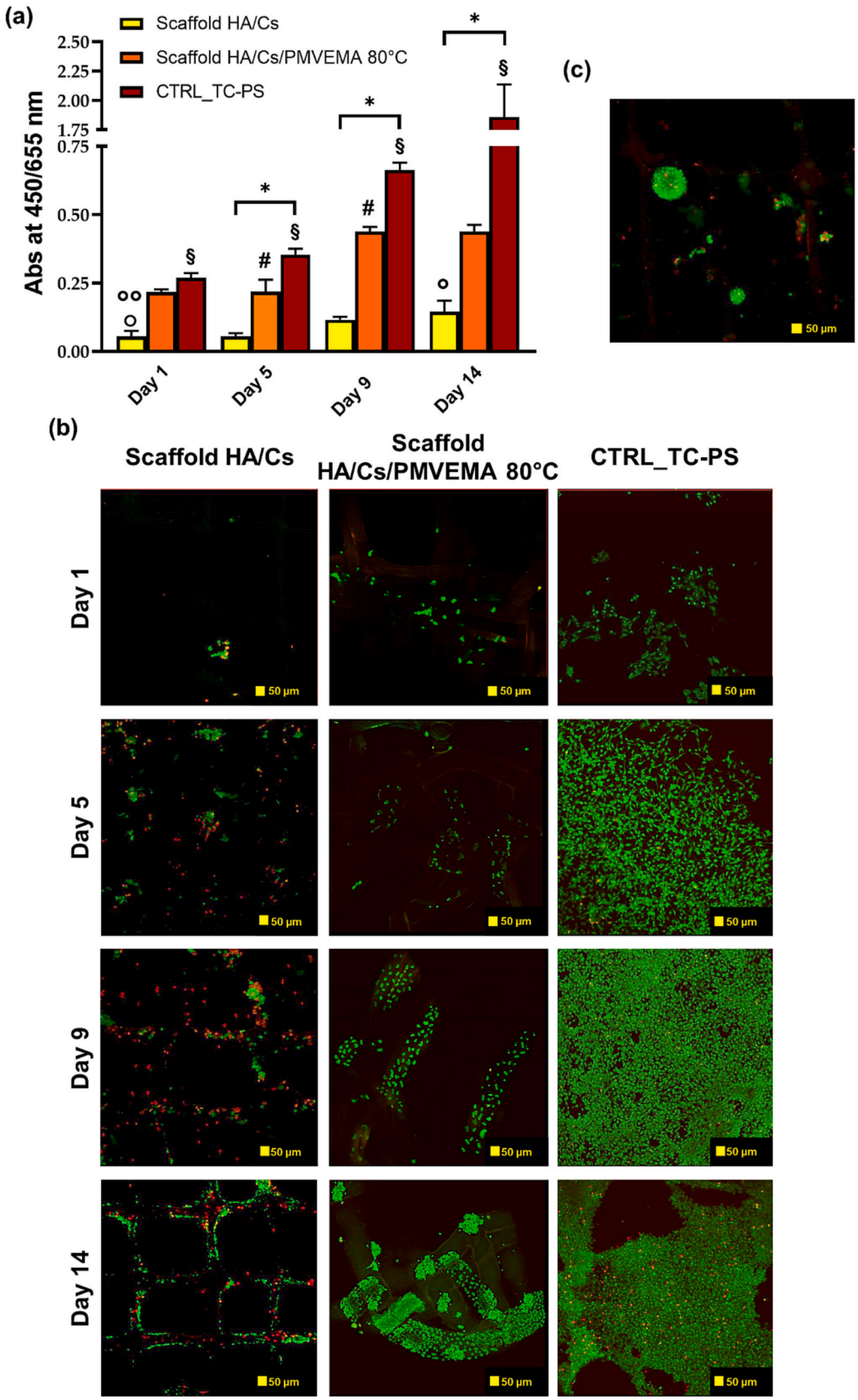

Fig. 10. Balb/3T3 clone A31 cell viability on HA/Cs scaffold, HA/Cs/PMVEMA 80 °C scaffold and TC-PS (control). (a) WST-1 assay; (b) Live/Dead assay; green channel depicts live cells, while red channel depicts dead cells (scale bar: 50 µm); (c) Live/Dead micrograph of cells grown on HA/Cs scaffold at day 9 of cell culture showing the formation of spheroids on the scaffold surface. Data are reported as mean ± standard deviation (n = 3). Data marked with the same symbol (°, # and §) are statistically different ($p < 0.05$). Data marked with * are statistically different at the same time point. Value marked with °° is statistically different from the others at the same time point ($p < 0.05$). (For interpretation of the references to color in this figure legend, the reader is referred to the web version of this article.)

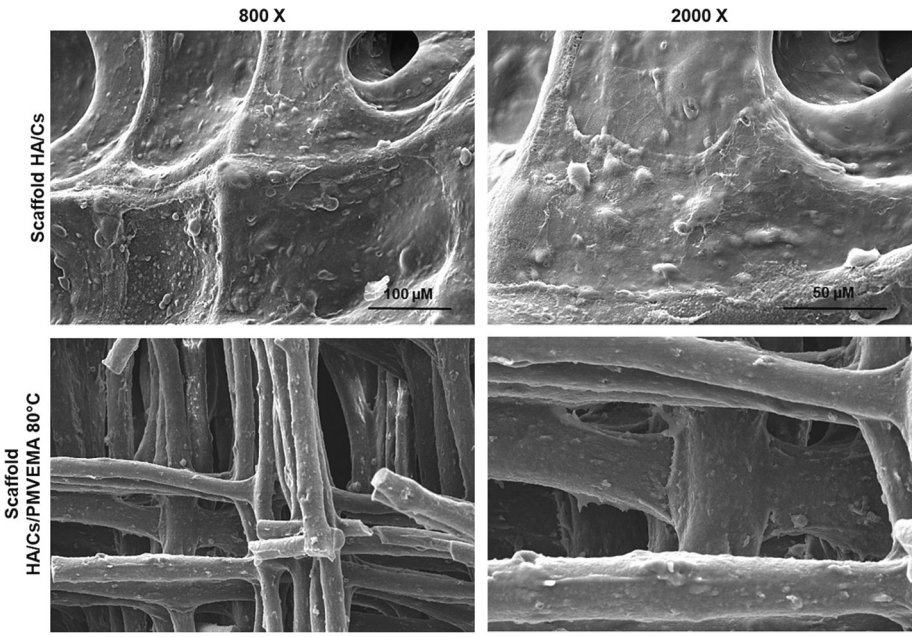

Fig. 11. Representative SEM micrographs of Balb/3T3 clone A31 cell/scaffold constructs at day 14 of cell culture (magnifications 800× and 2000×).

CRediT authorship contribution statement

Simona Braccini: Investigation, Methodology, Writing – original draft, Writing – review & editing. **Chong-Bo Chen:** Investigation, Methodology, Writing – original draft. **Jeannette Lucejko:** Investigation, Methodology, Writing – original draft. **Francesca Barsotti:** Investigation. **Claudia Ferrario:** Investigation. **Guo-Qiang Chen:** Conceptualization, Funding acquisition, Writing – review & editing. **Dario Puppi:** Conceptualization, Funding acquisition, Investigation, Methodology, Project administration, Resources, Supervision, Validation, Writing – original draft, Writing – review & editing.

Declaration of competing interest

The authors declare that they have no known competing financial interests or personal relationships that could have appeared to influence the work reported in this paper.

Data availability

Data will be made available on request.

Acknowledgments

This article is dedicated to the memory of Prof. Emo Chiellini, University of Pisa, who represented an endless source of inspiration for materials scientists. Part of the present study was financially supported by the European Commission (EC)-funded project 'Hyanji Scaffold' in the People Program of the 7FP. CISUP, the Centre for Instrumentation Sharing of the University of Pisa, is acknowledged for SEM, EGA-MS, and Py-GC/MS analysis. Randa Ishak is kindly acknowledged for the assistance during SEM analysis.

References

Andrade del Olmo, J., Alonso, J. M., Sáez Martínez, V., Ruiz-Rubio, L., Pérez González, R., Vilas-Vilela, J. L., & Pérez-Álvarez, L. (2021). Biocompatible hyaluronic acid-divinyl sulfone injectable hydrogels for sustained drug release with enhanced antibacterial properties against *Staphylococcus aureus*. *Materials Science and Engineering: C, 125*, Article 112102.

Boobphahom, S., Nguyet Ly, M., Soum, V., Pyun, N., Kwon, O.-S., Rodthongkum, N., & Shin, K. (2020). Recent advances in microfluidic paper-based analytical devices toward high-throughput screening. *Molecules, 25*(13).

Braccini, S., Tacchini, C., Chiellini, F., & Puppi, D. (2022). Polymeric hydrogels for in vitro 3D ovarian cancer modeling. *International Journal of Molecular Sciences, 23*(6).

Brodbeck, W. G., Patel, J., Voskerician, G., Christenson, E., Shive, M. S., Nakayama, Y., … Anderson, J. M. (2002). Biomaterial adherent macrophage apoptosis is increased by hydrophilic and anionic substrates in vivo. *Proceedings of the National Academy of Sciences, 99*(16), 10287–10292.

Brodbeck, W. G., Shive, M. S., Colton, E., Nakayama, Y., Matsuda, T., & Anderson, J. M. (2001). Influence of biomaterial surface chemistry on the apoptosis of adherent cells. *Journal of Biomedical Materials Research, 55*(4), 661–668.

Bucatariu, S.-M., Constantin, M., Varganici, C.-D., Rusu, D., Nicolescu, A., Prisacaru, I., … Fundueanu, G. (2020). A new sponge-type hydrogel based on hyaluronic acid and poly(methylvinylether-alt-maleic acid) as a 3D platform for tumor cell growth. *International Journal of Biological Macromolecules, 165*, 2528–2540.

Campoccia, D., Doherty, P., Radice, M., Brun, P., Abatangelo, G., & Williams, D. F. (1998). Semisynthetic resorbable materials from hyaluronan esterification. *Biomaterials, 19*(23), 2101–2127.

Cárdenas-Triviño, G., Ruiz-Parra, M., Vergara-González, L., Ojeda-Oyarzún, J., & Solorzano, G. (2017). Synthesis and bactericidal properties of hyaluronic acid doped with metal nanoparticles. *Journal of Nanomaterials, 2017*, Article 9573869.

Carneiro, J., Döll-Boscardin, P. M., Fiorin, B. C., Nadal, J. M., Farago, P. V., & Paula, J. P. d. (2016). Development and characterization of hyaluronic acid-lysine nanoparticles with potential as innovative dermal filling. *Brazilian Journal of Pharmaceutical Sciences, 52*(4), 645–651.

Chen, H., Qin, J., & Hu, Y. (2019). Efficient degradation of high-molecular-weight hyaluronic acid by a combination of ultrasound, hydrogen peroxide, and copper ion. *Molecules, 24*.

Chhabra, H., Gupta, P., Verma, P. J., Jadhav, S., & Bellare, J. R. (2014). Gelatin–PMVE/MA composite scaffold promotes expansion of embryonic stem cells. *Materials Science and Engineering: C, 37*, 184–194.

Chiellini, F., Puppi, D., Piras, A., Morelli, A., Bartoli, C., & Migone, C. (2016). Modelling of pancreatic ductal adenocarcinoma in vitro with three-dimensional microstructured hydrogels. *RSC Advances, 6*, 54226–54235.

Coimbra, P., Alves, P., Valente, T. A. M., Santos, R., Correia, I. J., & Ferreira, P. (2011). Sodium hyaluronate/chitosan polyelectrolyte complex scaffolds for dental pulp regeneration: synthesis and characterization. *International Journal of Biological Macromolecules, 49*(4), 573–579.

Correia, C. R., Moreira-Teixeira, L. S., Moroni, L., Reis, R. L., van Blitterswijk, C. A., Karperien, M., & Mano, J. F. (2011). Chitosan scaffolds containing hyaluronic acid for cartilage tissue engineering. *Tissue Engineering. Part C, Methods, 17*(7), 717–730.

Dahmane, E. M., Taourirte, M., Eladlani, N., & Rhazi, M. (2014). Extraction and characterization of chitin and chitosan from *Parapenaeus longirostris* from Moroccan local sources. *International Journal of Polymer Analysis and Characterization, 19*(4), 342–351.

Dash, M., Chiellini, F., Ottenbrite, R. M., & Chiellini, E. (2011). Chitosan—A versatile semi-synthetic polymer in biomedical applications. *Progress in Polymer Science, 36*(8), 981–1014.

de Sousa Victor, R., da Cunha, M., Santos, A., Viana de Sousa, B., de Araújo Neves, G., de Lima, N., … Rodrigues Menezes, R. (2020). A review on chitosan's uses as biomaterial: tissue engineering, drug delivery systems and cancer treatment. *Materials, 13*(21).

Demir, Y. K., Metin, A.Ü., Şatıroğlu, B., Solmaz, M. E., Kayser, V., & Mäder, K. (2017). Poly (methyl vinyl ether-co-maleic acid) – Pectin based hydrogel-forming systems: Gel, film, and microneedles. *European Journal of Pharmaceutics and Biopharmaceutics, 117*, 182–194.

Dhiman, M., Yedurkar, P., & Sawant, K. K. (2008). Formulation, characterization, and in vitro evaluation of bioadhesive gels containing 5-fluorouracil. *Pharmaceutical Development and Technology, 13*(1), 15–25.

Dovedytis, M., Liu, Z. J., & Bartlett, S. (2020). Hyaluronic acid and its biomedical applications: A review. *Engineered Regeneration, 1*, 102–113.

Fernandes Queiroz, M., Melo, K. R., Sabry, D. A., Sassaki, G. L., & Rocha, H. A. (2015). Does the use of chitosan contribute to oxalate kidney stone formation? *Marine Drugs, 13*, 141–158.

Finnberg, N. K., Gokare, P., Lev, A., Grivennikov, S. I., MacFarlane Iv, A. W., Campbell, K. S., … El-Deiry, W. S. (2017). Application of 3D tumoroid systems to define immune and cytotoxic therapeutic responses based on tumoroid and tissue slice culture molecular signatures. *Oncotarget, 8*(40), 66747–66757.

Florczyk, S. J., Wang, K., Jana, S., Wood, D. L., Sytsma, S. K., Sham, J. G., … Zhang, M. (2013). Porous chitosan-hyaluronic acid scaffolds as a mimic of glioblastoma microenvironment ECM. *Biomaterials, 34*(38), 10143–10150.

Gierszewska, M., & Ostrowska-Czubenko, J. (2016). Equilibrium swelling study of crosslinked chitosan membranes in water, buffer and salt solutions. *Progress on Chemistry and Application of Chitin and its Derivatives, 21*, 55–62.

Goetz, L., Foston, M., Mathew, A. P., Oksman, K., & Ragauskas, A. J. (2010). Poly(methyl vinyl ether-co-maleic acid)−polyethylene glycol nanocomposites cross-linked in situ with cellulose nanowhiskers. *Biomacromolecules, 11*(10), 2660–2666.

Gómez, S., Gamazo, C., Roman, B. S., Ferrer, M., Sanz, M. L., & Irache, J. M. (2007). Gantrez® AN nanoparticles as an adjuvant for oral immunotherapy with allergens. *Vaccine, 25*(29), 5263–5271.

Gómez, S., Gamazo, C., Roman, B. S., Vauthier, C., Ferrer, M., & Irache, J. M. (2006). Development of a novel vaccine delivery system based on Gantrez nanoparticles. *Journal of Nanoscience and Nanotechnology, 6*(9–10), 3283–3289.

Hamedi, H., Moradi, S., Tonelli, A. E., & Hudson, S. M. (2019). Preparation and characterization of chitosan–alginate polyelectrolyte complexes loaded with antibacterial thyme oil nanoemulsions. *Applied Sciences, 9*(18).

Han, L., Zhao, Y., Yin, L., Li, R., Liang, Y., Huang, H., … Feng, M. (2012). Insulin-loaded pH-sensitive hyaluronic acid nanoparticles enhance transcellular delivery. *AAPS PharmSciTech, 13*(3), 836–845.

Islam, M. M., Shahruzzaman, M., Biswas, S., Nurus Sakib, M., & Rashid, T. U. (2020). Chitosan based bioactive materials in tissue engineering applications-A review. *Bioactive Materials, 5*(1), 164–183.

ISO 10993-5. (2009). *Biological evaluation of medical devices — Part 5: Tests for in vitro cytotoxicity*.

Jennings, J. A. (2017). 7 - Controlling chitosan degradation properties in vitro and in vivo. In J. A. Jennings, & J. D. Bumgardner (Eds.), *Vol. 1. Chitosan based biomaterials* (pp. 159–182). Woodhead Publishing.

Jia, Y., Huo, M., Huang, H., Fu, W., Wang, Y., Zhang, J., & Jia, S. (2015). Preparation and characterization of bacterial cellulose/hyaluronic acid composites. *Proceedings of the Institution of Mechanical Engineers, Part N: Journal of Nanomaterials, Nanoengineering and Nanosystems, 229*(1), 41–48.

Jiménez-Gómez, C. P., & Cecilia, J. A. (2020). Chitosan: A natural biopolymer with a wide and varied range of applications. *Molecules, 25*.

Jung, H. (2020). Hyaluronidase: An overview of its properties, applications, and side effects. *Archives of Plastic Surgery, 47*(4), 297–300.

Kim, S. J., Shin, S. R., Lee, K. B., Park, Y. D., & Kim, S. I. (2004). Synthesis and characteristics of polyelectrolyte complexes composed of chitosan and hyaluronic acid. *Journal of Applied Polymer Science, 91*(5), 2908–2913.

Kwon, M. Y., Wang, C., Galarraga, J. H., Puré, E., Han, L., & Burdick, J. A. (2019). Influence of hyaluronic acid modification on CD44 binding towards the design of hydrogel biomaterials. *Biomaterials, 222*, Article 119451.

Laizure, S. C., Herring, V., Hu, Z., Witbrodt, K., & Parker, R. B. (2013). The role of human carboxylesterases in drug metabolism: Have we overlooked their importance? *Pharmacotherapy, 33*(2), 210–222.

Larrañeta, E., Henry, M., Irwin, N. J., Trotter, J., Perminova, A. A., & Donnelly, R. F. (2018). Synthesis and characterization of hyaluronic acid hydrogels crosslinked using a solvent-free process for potential biomedical applications. *Carbohydrate Polymers, 181*, 1194–1205.

Lewandowska, K., Sionkowska, A., Grabska, S., & Michalska, M. (2017). Characterisation of chitosan/hyaluronic acid blend films modified by collagen. *Progress on Chemistry and Application of Chitin and its Derivatives, 22*, 125–134.

Li, H., Tan, C., & Li, L. (2018). Review of 3D printable hydrogels and constructs. *Materials & Design, 159*, 20–38.

Li, J., Wu, C., Chu, P. K., & Gelinsky, M. (2020). 3D printing of hydrogels: Rational design strategies and emerging biomedical applications. *Materials Science & Engineering R: Reports, 140*, Article 100543.

Li, X., Xie, H., Lin, J., Xie, W., & Ma, X. (2009). Characterization and biodegradation of chitosan–alginate polyelectrolyte complexes. *Polymer Degradation and Stability, 94*(1), 1–6.

Ma, J., Wang, H., He, B., & Chen, J. (2001). A preliminary in vitro study on the fabrication and tissue engineering applications of a novel chitosan bilayer material as a scaffold of human neofetal dermal fibroblasts. *Biomaterials, 22*(4), 331–336.

Maiz-Fernández, S., Barroso, N., Pérez-Álvarez, L., Silván, U., Vilas-Vilela, J. L., & Lanceros-Mendez, S. (2021). 3D printable self-healing hyaluronic acid/chitosan polycomplex hydrogels with drug release capability. *International Journal of Biological Macromolecules, 188*, 820–832.

Manju, S., & Sreenivasan, K. (2011). Conjugation of curcumin onto hyaluronic acid enhances its aqueous solubility and stability. *Journal of Colloid and Interface Science, 359*(1), 318–325.

Martins, A. F., Pereira, A. G. B., Fajardo, A. R., Rubira, A. F., & Muniz, E. C. (2011). Characterization of polyelectrolytes complexes based on N,N,N-trimethyl chitosan/heparin prepared at different pH conditions. *Carbohydrate Polymers, 86*(3), 1266–1272.

Morelli, A., Puppi, D., & Chiellini, F. (2013). Polymers from renewable resources. *Journal of Renewable Materials, 1*(2), 83–112.

Morelli, A., Puppi, D., & Chiellini, F. (2017). Polysaccharide-based polyelectrolyte complexes for biomedical applications. In M. Koller (Ed.), *Current advances in biopolymer processing and characterization* (pp. 93–112). Nova Publishers.

Muzzarelli, R. A. A., Greco, F., Busilacchi, A., Sollazzo, V., & Gigante, A. (2012). Chitosan, hyaluronan and chondroitin sulfate in tissue engineering for cartilage regeneration: A review. *Carbohydrate Polymers, 89*(3), 723–739.

Nair, S. S., Zhu, J. Y., Deng, Y., & Ragauskas, A. J. (2014). Hydrogels prepared from cross-linked nanofibrillated cellulose. *ACS Sustainable Chemistry & Engineering, 2*(4), 772–780.

Nath, S. D., Abueva, C., Kim, B., & Lee, B. T. (2015). Chitosan–hyaluronic acid polyelectrolyte complex scaffold crosslinked with genipin for immobilization and controlled release of BMP-2. *Carbohydrate Polymers, 115*, 160–169.

Nitta, S. K., & Numata, K. (2013). Biopolymer-based nanoparticles for drug/gene delivery and tissue engineering. *International Journal of Molecular Sciences, 14*(1), 1629–1654.

Notario-Pérez, F., Martín-Illana, A., Cazorla-Luna, R., Ruiz-Caro, R., & Veiga, M. D. (2022). Applications of chitosan in surgical and post-surgical materials. *Marine Drugs, 20*(6).

Osório, L. A., Silva, E., & Mackay, R. E. (2021). A review of biomaterials and scaffold fabrication for organ-on-a-Chip (OOAC) systems. *Bioengineering, 8*(8), 113.

P, L., Skariyachan, S., & Bs, H. T. (2021). Cytotoxic effects of butyric acid derivatives through GPR109A receptor in Colorectal Carcinoma cells by in silico and in vitro methods. *Journal of Molecular Structure, 1243*, Article 130832.

Piras, A. M., Maisetta, G., Sandreschi, S., Esin, S., Gazzarri, M., Batoni, G., & Chiellini, F. (2014). Preparation, physical–chemical and biological characterization of chitosan nanoparticles loaded with lysozyme. *International Journal of Biological Macromolecules, 67*, 124–131.

Polexe, R. C., & Delair, T. (2013). Elaboration of stable and antibody functionalized positively charged colloids by polyelectrolyte complexation between chitosan and hyaluronic acid. *Molecules, 18*, 8563–8578.

Puppi, D., Braccini, S., Ranaudo, A., & Chiellini, F. (2020). Poly(3-hydroxybutyrate-co-3-hydroxyexanoate) scaffolds with tunable macro- and microstructural features by additive manufacturing. *Journal of Biotechnology, 308*, 96–107.

Puppi, D., & Chiellini, F. (2021). Computer-aided wet-spinning. In A. Rainer, & L. Moroni (Eds.), *Computer-aided tissue engineering: Methods and protocols* (pp. 101–110). New York, NY: Springer US.

Puppi, D., Chiellini, F., Piras, A., & Chiellini, E. (2010). Polymeric materials for bone and cartilage repair. *Progress in Polymer Science, 35*, 403–440.

Puppi, D., Migone, C., Morelli, A., Bartoli, C., Gazzarri, M., Pasini, D., & Chiellini, F. (2016). Microstructured chitosan/poly(γ-glutamic acid) polyelectrolyte complex hydrogels by computer-aided wet-spinning for biomedical three-dimensional scaffolds. *Journal of Bioactive and Compatible Polymers, 31*(5), 531–549.

Puppi, D., Mota, C., Gazzarri, M., Dinucci, D., Gloria, A., Myrzabekova, M., … Chiellini, F. (2012). Additive manufacturing of wet-spun polymeric scaffolds for bone tissue engineering. *Biomedical Microdevices, 14*(6), 1115–1127.

Rivero, R. E., Capella, V., Liaudat, A. C., Bosch, P., Barbero, C. A., & Rodr, N. (2020). Mechanical and physicochemical behavior of a 3D hydrogel scaffold during cell growth and proliferation. *RSC Advances, 10*, 5827–5837.

Salas, S., Talero, B., Rabasco, A. M., & González-Rodríguez, M. L. (2008). Development and validation of a reverse-phase liquid chromatographic method for the assay of lidocaine hydrochloride in alginate-Gantrez® microspheres. *Journal of Pharmaceutical and Biomedical Analysis, 47*(3), 501–507.

Sanad, R. A.-B., & Abdel-Bar, H. M. (2017). Chitosan–hyaluronic acid composite sponge scaffold enriched with Andrographolide-loaded lipid nanoparticles for enhanced wound healing. *Carbohydrate Polymers, 173*, 441–450.

Shu, X. Z., Liu, Y., Palumbo, F., & Prestwich, G. D. (2003). Disulfide-crosslinked hyaluronan-gelatin hydrogel films: A covalent mimic of the extracellular matrix for in vitro cell growth. *Biomaterials, 24*(21), 3825–3834.

Sood, A., Gupta, A., & Agrawal, G. (2021). Recent advances in polysaccharides based biomaterials for drug delivery and tissue engineering applications. *Carbohydrate Polymer Technologies and Applications, 2*, Article 100067.

Suo, L., Xue, Z., Wang, P., Wu, H., Chen, Y., & Shen, J. (2022). Improvement of osteogenic properties using a 3D-printed graphene oxide/hyaluronic acid/chitosan composite scaffold. *Journal of Bioactive and Compatible Polymers, 37*(4), 267–283.

Tiwari, S., & Bahadur, P. (2019). Modified hyaluronic acid based materials for biomedical applications. *International Journal of Biological Macromolecules, 121*, 556–571.

Turner, N. J., Kielty, C. M., Walker, M. G., & Canfield, A. E. (2004). A novel hyaluronan-based biomaterial (Hyaff-11®) as a scaffold for endothelial cells in tissue engineered vascular grafts. *Biomaterials, 25*(28), 5955–5964.

Wang, Q. Z., Chen, X. G., Liu, N., Wang, S. X., Liu, C. S., Meng, X. H., & Liu, C. G. (2006). Protonation constants of chitosan with different molecular weight and degree of deacetylation. *Carbohydrate Polymers, 65*(2), 194–201.

Yamane, S., Iwasaki, N., Majima, T., Funakoshi, T., Masuko, T., Harada, K., Minami, A., Monde, K., & Nishimura, S.-I. (2005). Feasibility of chitosan-based hyaluronic acid hybrid biomaterial for a novel scaffold in cartilage tissue engineering. *Biomaterials, 26*(6), 611–619.

Yamanlar, S., Sant, S., Boudou, T., Picart, C., & Khademhosseini, A. (2011). Surface functionalization of hyaluronic acid hydrogels by polyelectrolyte multilayer films. *Biomaterials, 32*(24), 5590–5599.

Yao, Z.-Y., Qin, J., Gong, J.-S., Ye, Y.-H., Qian, J.-Y., Li, H., Xu, Z.-H., & Shi, J.-S. (2021). Versatile strategies for bioproduction of hyaluronic acid driven by synthetic biology. *Carbohydrate Polymers, 264*, Article 118015.

Yoncheva, K., Lizarraga, E., & Irache, J. M. (2005). Pegylated nanoparticles based on poly(methyl vinyl ether-co-maleic anhydride): Preparation and evaluation of their bioadhesive properties. *European Journal of Pharmaceutical Sciences, 24*(5), 411–419.

Zhang, R., Chang, S. J., Jing, Y., Wang, L., Chen, C.-J., & Liu, J.-T. (2023). Application of chitosan with different molecular weights in cartilage tissue engineering. *Carbohydrate Polymers, 314*, Article 120890.

Zhang, T., Chen, J., Zhang, Q., Dou, J., & Gu, N. (2013). Poly(ethylene glycol)-cross linked poly(methyl vinyl ether-co-maleic acid)hydrogels for three-dimensional human ovarian cancer cell culture. *Colloids and Surfaces A: Physicochemical and Engineering Aspects, 422*, 81–89.